Fluorescence imaging of *Drosophila melanogaster* tracheal system: investigating the morphology of LUBEL mutant flies

Sabrina Benoit

42001, sabrina.benoit@abo.fi

Master's thesis

Master's Degree Program in Biomedical Imaging

Faculty of Science and Engineering

Åbo Akademi University, Turku

Supervisors:

Annika Meinander, Docent, PhD

Anna Aalto, MSc, PhD student

July 2020

Turku, Finland

Benoit, Sabrina

Abstract

Åbo Akademi University
Master's Degree Program in Biomedical Imaging
Faculty of Science and Engineering

NAME OF THE STUDENT:
Sabrina Benoit

Title of the thesis:
Fluorescence imaging of Drosophila melanogaster tracheal system: investigating the morphology of LUBEL mutant flies

Ubiquitination is a post-translational modification that is a key regulator in many pathways in the cell. Mutant LUBEL (*lubel^Mi*), linear ubiquitin E3 ligase, flies are unable to form methionine 1 (M1) linked ubiquitin chains in *Drosophila* and die in hypoxic conditions, whereas wild-type *Canton^s* flies survive. The *Drosophila* respiratory system is examined to determine if the flies are asphyxiating due to morphological changes in the tracheal epithelial tissue. To image morphological changes in the epithelial tissue, I used chitin-specific and tubulin-specific silicone rhodamine (SiR) probes and Calcofluor White staining in combination with Zeiss LSM 880 with AiryScan microscopy techniques to evaluate the respiratory system in *Canton^S* in basal conditions, and, thus, develop a criterion for comparison with *lubel^Mi* flies. I then used STED microscopy to image taenidia within the tracheoles and measure tracheole diameter in *Canton^S* and *lubel^Mi* flies. A novel phenotypic abnormality was seen in LUBEL mutant flies, *lubel^Mi* and *lubel^RNAi* flies, in comparison to the control group. *lubel^Mi* and *lubel^RNAi* flies have discontinuous, abnormal tubulin projecting from the trachea and tracheoles and measurably thicker dorsal trunks in comparison to the control group. This abnormal tubulin phenotype and increased dorsal trunk diameter could be caused by a LUBEL-influenced developmental error during organogenesis in *Drosophila melanogaster* larvae.

KEYWORDS: ubiquitination, LUBEL, *Drosophila*, trachea, tubulin

LIST OF ABBREVIATIONS

3D- three dimensional
AMP- anti-microbial peptides
CCD- charge couple detectors
COOH- carboxylic acid
COPD- chronic obstructive pulmonary disease
DIF- dorsal-related immunity factor
DNA- deoxyribonucleic acid
E1- ubiquitin-activating enzyme
E2- ubiquitin-conjugating enzyme
E3- ubiquitin-protein ligases
HOIP- HOIL-1-interacting protein
IR- infrared
LDH- lactate dehydrogenase
LED- light emitting diode
LUBAC- linear ubiquitin chain assembly complex
LUBEL- linear ubiquitin E3 ligase
M1- methionine 1
MT- microtubule
NA- numerical aperture
NF-κB- nuclear factor kappa B
nm- nanometers
PMT- photomultiplier tube
PTM- post-translational modification
sCMOS- scientific complementary metal oxide semiconductors
SiR- silicone rhodamine
STED-stimulated emission depletion
TF- transcription factor
Ub- ubiquitin
UBD- ubiquitin D
UV- ultraviolet

Table of Contents

1. LITERATURE OVERVIEW

1.1 Microscopy

The first microscopes date back to the 13th century, starting as a single lens magnifying glass and later developing into more sophisticated devices, such as the compound microscope. The word microscope derives from Ancient Greek words mikrós, meaning "small", and skopéō meaning, "to look at" (Bardell, 2004*).* The growing field of microscopy has allowed scientists to view objects otherwise unseen by the human eye, such as cells, viruses, and other small structures, such as the *Drosophila melanogaster* respiratory system.

1.2 Fluorescence

Fluorescence is a form of luminescence that is caused by the excitation of an electron. The electron excitation subsequently causes the emission of a photon which produces light. An electron can be excited physically through the absorption of light, mechanically by forces such as friction, or through chemical reactions. In regard to microscopy, the electrons of a fluorophore are excited to the singlet state (S_1 and S_2) by the absorption of light within a specific wavelength and as the electron returns to the ground state (S_0), a photon is emitted within a specific wavelength (Figure 1) (Lakowicz, 2006).
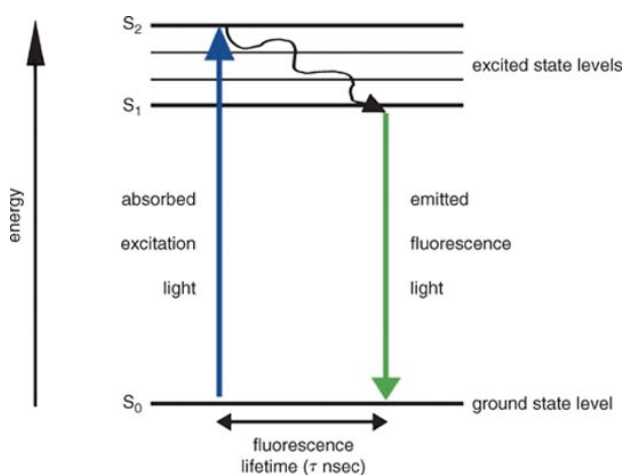
Figure 1. Photon excitation from ground state level to excited state level due to the absorption of electromagnetic waves within the photon's excitation spectrum. As the photon vibrates and releases energy, it steps down from the S2 excited state level to the S1 excited state level and light is emitted from the photon as it returns to the ground state level.

The average lifetime of a fluorophore (time between excitation and proton emission) is

around 10 ns. Luminescence can also have longer lifetimes; this is known as phosphorescence. During phosphorescence, the proton emission occurs as an electron slowly returns to ground state from the triplet state (T_1) generating lifetimes of milliseconds to seconds (Figure 2) (Fister et al., 1997).
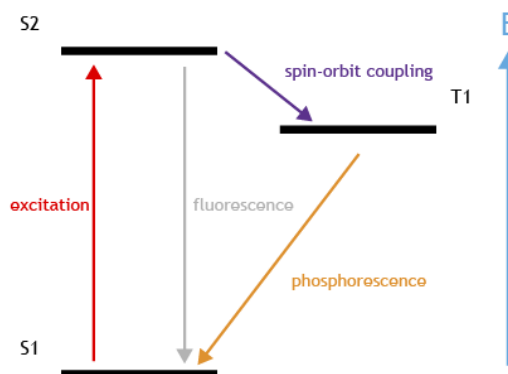
Figure 2. Phosphorescence occurs when a photon undergoes spin-orbit coupling which sends it into the triplet state. There is a time delay when returning to the ground state level from the triplet state, causing phosphorescence light emission.

The unique properties of aromatic fluorophores in combination with larger macromolecules such as lipids, enzymes, or proteins, constitute fluorochromes that are capable of undergoing electron transitions in biological systems (Herman et al., 2015). Fluorochromes are excited by light within a specific wavelength range and the emission occurs within an increasing wavelength range, this is called the Stokes' shift (Figure 3). Stokes' shift is defined as the difference between the maximum excitation wavelength and the maximum emission wavelength (Fister et al., 1997).

6
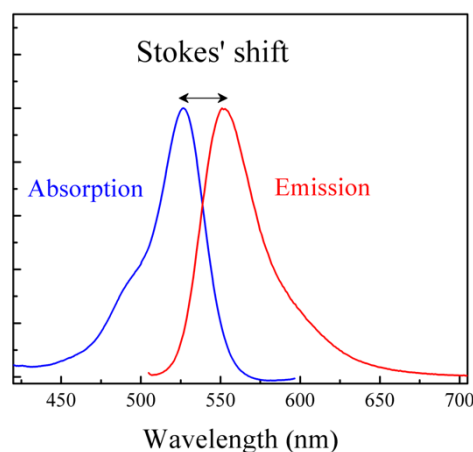
Figure 3. Stokes' shift is characterized by the wavelength difference between the absorption and emission spectrums of a photon. When a photon is returning to the ground state level after excitation there is a vibrational loss of energy. This loss of energy causes a shift in the wavelength of the emission light because light of longer wavelengths has lower energy levels.

After an electron is excited to the singlet state due to the absorption of a photon, the electron must relax to the ground state through the emission of a photon and vibrational relaxation, which causes a loss of energy. Decreasing energy causes an increase in the photon's wavelength, thus a change in visible light color (Thermofisher Scientific, 2017). E.g. A fluorochrome excited by light within 450-550 nm (green) will emit light between 550-650 nm (yellow/orange) (Figure 4).
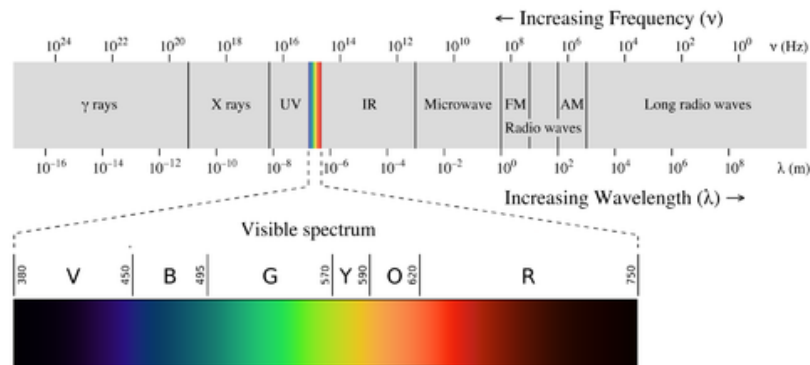

Figure 4. Fluorophores can be excited by electromagnetic waves ranging from ultraviolet waves (UV) to infrared waves (IR). As electromagnetic waves increase in wavelength, they decrease in energy. Visible light exists between the wavelengths 380-750 nm, and fluorophores used in microscopy emit light within the visible light spectrum.

The Stokes' shift is crucial for the use of fluorochromes in microscopy. Fluorochromes can be conjugated with certain macromolecules that allow them to attach to specific biological structures with strong specificity. By using specific light sources, excitation and emission filters, and specialized detectors, one can excite the fluorochrome and detect the emitted photons to visualize the location, function, or structure of the target of interest (Herman et al., 2015).

1.2.1 Silicon Rhodamine Fluorophores

There is a specific family of fluorophores known as rhodamines. Within this family is a newly developed derivative: an organic fluorophore known as silicone rhodamine (SiR). During the development of the SiR probes, the intended use was for live-cell imaging; therefore, they were originally developed to target the two primary components of the cytoskeleton: tubulin and actin. The SiR probes were conjugated to the microtubule and F-actin ligands docetaxel and desbromo-demethyl-jasplakinolide (Lukinavičius et al., 2014). SiR is an ideal fluorophore because it is bright, highly fluorogenic and photostable. SiR excitation and emission wavelengths are in the far-red spectral range (650-670 nm) where little autofluorescence and phototoxicity occurs. These longer wavelength values and lower energy levels of the far-red light allow for more gentle and deeper penetration into the samples (Lukinavičius et al., 2013). SiR staining does not require any transfection or washing steps, which is ideal for staining small, delicate structures. When moving delicate tissue samples from one solution to another, the surface tension of the liquid solution breaks and damages the tissue, regardless of how carefully the tissue is transferred (Pitsch and Köster, 2015).

SiR derivates exist in equilibrium between the fluorescent ON state and nonfluorescent OFF state. SiR is conjugated to a ligand that specifically binds to a target of interest (e.g. tubulin). For example, the ligand binds to the polar target surface of tubulin, hydrophobic aggregation occurs, causing a conformational change of the conjugated SiR probe. The probe exists in a closed, spirolactone form until it binds to the polar protein surface and changes to an open, zwitterion form that is excitable by far-red light (Pitsch and Köster, 2015).

Spirochrome, the producer of SiR fluorophores, have since developed many different versions of SiR labelling, such as SiR- DNA labelling, SiR F-actin labelling, and SiR-COOH staining. When SiR-COOH was colocalized with Calcofluor white staining in *Drosophila melanogaster* larvae, a bright staining signal was seen, indicating that SiR-COOH can be used to stain chitin-composed taenidia in the respiratory system (Lukinavičius et al., 2013). Calcofluor white is an easy-to-use, well-validated fluorescence dye that specifically binds to chitin and cellulose. Calcofluor white, like SiR, can be used without any transfection or washing steps, making it an ideal companion to SiR when staining the respiratory system in *Drosophila* (Lukinavičius et al., 2018).

1.3 Fluorescence microscopy

Microscopy in combination with specialized chemical compounds, known as fluorophores, allows one to view specifically illuminated structures within a microscopic organism. This is known as fluorescence microscopy. Fluorescence microscopy is used to visualize target structures by detecting the fluorescence emitted by a fluorophore-tagged sample. Some example of fluorescence microscopes include laser scanning confocal microscopes, spinning disk microscopes, two-photon microscopes, and super-resolution microscopes (Sanderson et al., 2014*).*
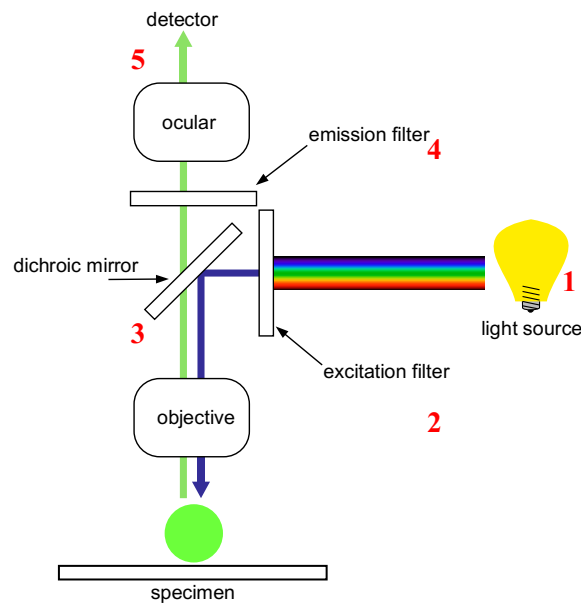
Figure 5. Schematic diagram of a fluorescence microscope. A basic fluorescence microscope has five primary components: light source, excitation filter, dichroic mirror, emission filter, and detector.

Basic setup of a fluorescence microscope (depicted in Fig. 5):

1. *Light source*: A light source must be used to illuminate the sample and excite the fluorochromes. A variety of light sources can be used for fluorescence microscopes, similarly to a basic compound microscope. Some examples of commonly used light sources include mercury lamps, xenon lamps, argon lasers, light-emitting diode (LED).

2. *Excitation filter*: In order to ensure that we are visualizing the target of interest, only light within the specific excitation range should be projected onto the sample; this also reduces the amount of light and phototoxic energy that the fluorochrome is being exposed to. Excitation filters allow only light within a specific excitation

wavelength range to pass through it and all other wavelengths of light are blocked out.

3. *Dichroic mirror*: Dichroic mirrors, or dichromatic beam splitters, control the movement and reflection of light within the microscope. Using specialized glass coating and interference filters, only light within the excitation spectra is reflected onto the objective, while only light within the emission spectra is allowed to pass through the dichroic mirror towards the detector.

4. *Emission filter*: Before the emitted light from the sample enters the detector, it must first pass through an emission filter. Similar to the excitation filter, the emission filter only allows light within a specific emission wavelength range to pass through it and all other wavelengths of light are blocked out.

5. *Detector*: After passing through the emission filter, the light is directed into the eyepiece for viewing by the operator or into the detector. Monochromatic cameras with high sensitivity and low noise are the most commonly used form of detector. The two main types of camera detectors are CCD (Charge Coupled Detectors) and sCMOS (scientific Complementary Metal Oxide Semiconductors) (Mandracchia et al., 2020).

1.3.1 Confocal Microscopy

Confocal microscopy is a fluorescence microscopy technique that uses a pinhole to block out-of-focus light from reaching the detector, thus improving image resolution and contrast. When light passes through a pinhole, an airy disk forms. An airy disk is the name of the bright, central region of the diffraction pattern that is produced when light passes through a small circular aperture, such as a pinhole (Airy, 1835). There are two main types of confocal microscopy that utilize this pinhole technique: laser scanning confocal microscope and spinning disk confocal microscope.

Laser scanning confocal microscopy is fundamentally similar to a basic widefield fluorescence microscope. A light source (laser) with a specific wavelength within the excitation spectra of a fluorophore is used to illuminate the sample. The light source reflects off of a dichroic mirror and, in a widefield fluorescence microscope, the light source would directly illuminate the sample. However, in laser scanning confocal microscopy, the laser strikes motorized mirrors that then scan the laser across the sample (Prasad et al., 2007). Spinning disk confocal microscopy utilizes the same pinhole principle as laser confocal microscopy, but in spinning disk microscopy, the microscope

is able to detect multiple points simultaneously by using a spinning disk with multiple pinholes versus a narrow scanning laser and one pinhole. After the absorption of the scanned light and excitation of the fluorochrome, emission light passes through the dichroic mirror and is focused through the pinhole, and this focused light is then detected by the detector. As the microscope scans the sample with the excitation laser, the sample is being interpreted bit by bit, pixel by pixel. After the emission photons are detected by the detector (usually a photomultiplier tube), computer software uses the pixels to create the overall image (Prasad et al., 2007).
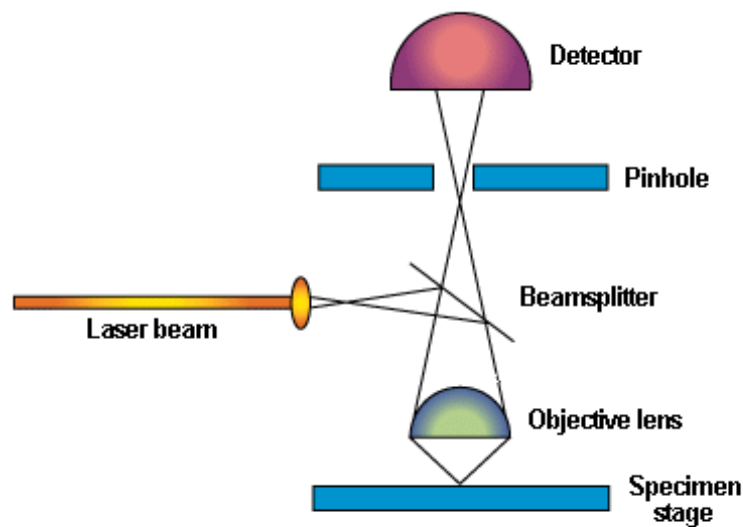
Figure 6. The basic setup of a confocal scanning light microscope has six primary components: detector, pinhole, light source (laser beam), beamsplitter, objective lens, and specimen stage. The light source is scanned across the sample using a system of motorized mirrors (beamsplitter) and the emission light passes through a pinhole to reduce outside noise before reaching the detector.

Photomultiplier tubes is an extremely photosensitive device that releases an electron in response to the absorption of a photo. As a photon passes through the photocathode, an electron is then released. This electron is then multiplied as it is traveling across the tube and strikes the dynode chain. Once the electrons have traveled across the tube and multiplied the signal, an anode collects the multiplied electrons and generates a detectable current. Photomultiplier tubes are an essential component of a laser scanning confocal microscope because the microscope only scans one pixel of the sample at a time; therefore, a very sensitive detector is required to generate an image (Abramowitz and Davidson, 1999).

Figure 7. Photomultiplier tubes (PMT) release an electron from the photocathode upon contact with a photon. The electron travels across the dynode chain, causing a release of additional electrons, which amplifies the signal given from one single photon. This signal amplification makes PMTs a preferred form of photon detection due to its sensitivity.
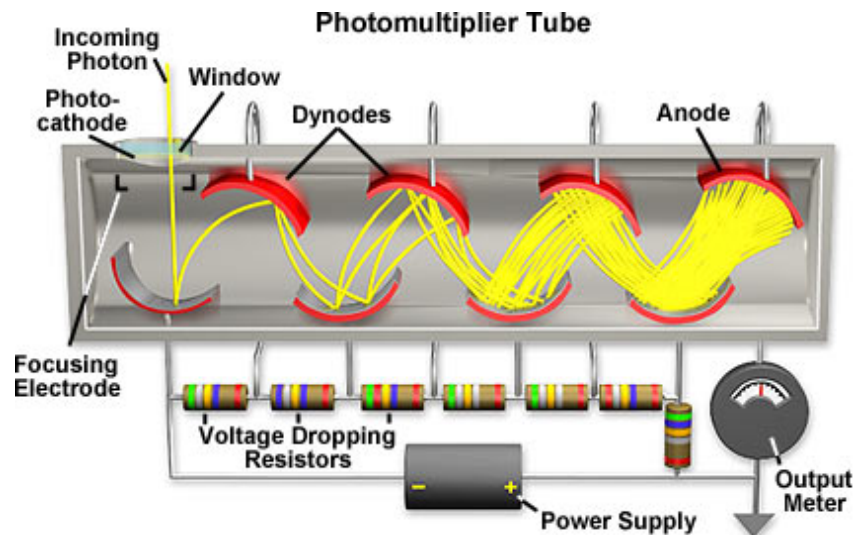
Confocal microscopy techniques have greatly improved the field of fluorescence microscopy by its ability to reduce out of focus light and create 3D images using optical sectioning. Not only does this reduce the amount of damaging light that the sample is exposed to, but also creates images with reduced background noise due to the use of a pinhole to only collect focused light. Stimulated emission depletion (STED) microscopy is a super-resolution, fluorescence microscopy technique that uses an additional depletion laser to reduce fluorescence emission surrounding the focal point within a sample (Gines and Davidson. 2018). Before the development of super-resolution microscopes, the resolution of a microscope was defined by the Abbe diffraction limit for a microscope:

$$d = \frac{\lambda}{2n \sin \theta} = \frac{\lambda}{2NA}$$

The diffraction limit of a microscope is dependent upon the traveling light wavelength (λ) and the numerical aperture (NA) of the microscope's objective. This defines the resolution limit: the distance at which the microscope can completely distinguish between two separate points within a sample (~200 nm). STED microscopy was developed in order to overcome this resolution limitation of previous confocal microscopes. When a single point is excited within a sample, an Airy disk forms within the diffraction pattern of the emission light. The volume of excitation light is larger than

the size of the actual point, which restricts the microscope's ability to distinguish two closely located points from one another. STED microscopy uses a donut-shaped depletion laser to shrink the excitation area surrounding the focal point through the deactivation of fluorophores in the outer regions of the Airy disk, allowing images to be resolved beyond 200 nm (Figure 8) (Gines and Davidson. 2018).
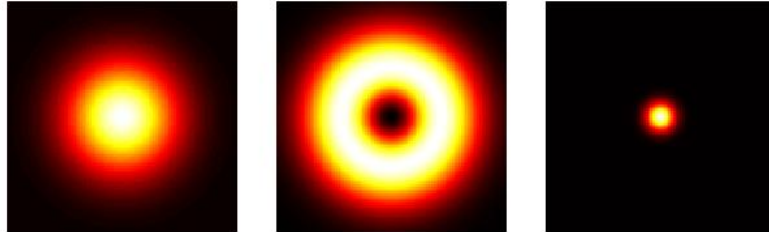
Figure 8. Effect of a STED depletion laser on an excitation beam. Excitation beam exciting a focus point (left), donut-shaped depletion laser (middle), and the remaining fluorescence emission once the two lasers are merged (right).

In a traditional fluorescence microscope, a fluorophore is excited by a light source within its excitation wavelength range by the absorption of a photon. This absorption causes an electron of the fluorophore to jump from ground state to singlet state. After excitation, the electron relaxes to the ground state and releases its energy as a photon with a specific emission wavelength. In STED, this process is interrupted before the electron can relax and release a photon. The excited electron is hit with a high intensity depletion laser, which forces it to relax to the ground energy level, thus inactivating the fluorophore (Figure 9) (Gines and Davidson. 2018).

Figure 9. Jablonski diagram representation of an electron's stimulated emission. In comparison to traditional confocal microscopy fluorescence emission, stimulated emission of a photon causes a decrease in energy and increase in wavelength (redshift).

In a STED microscope setup, the light source is composed of two synchronized pulsed lasers (excitation and depletion lasers). The depletion laser passes through a phase plate, which causes the laser's donut-like shape. Both lasers pass through dichroic mirrors, similarly to confocal mi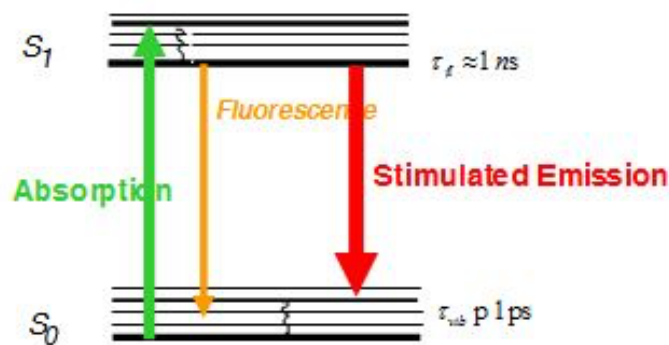croscopy, that allows excitation light to be reflected onto the sample, and emission light to pass through the dichroic mirror and enter the detector (photo-multiplier tube). Unlike confocal microscopy, STED microscopes have fixed laser paths and a scanning sample stage versus a scanning laser (Figure 10) (Gines and Davidson, 2018).
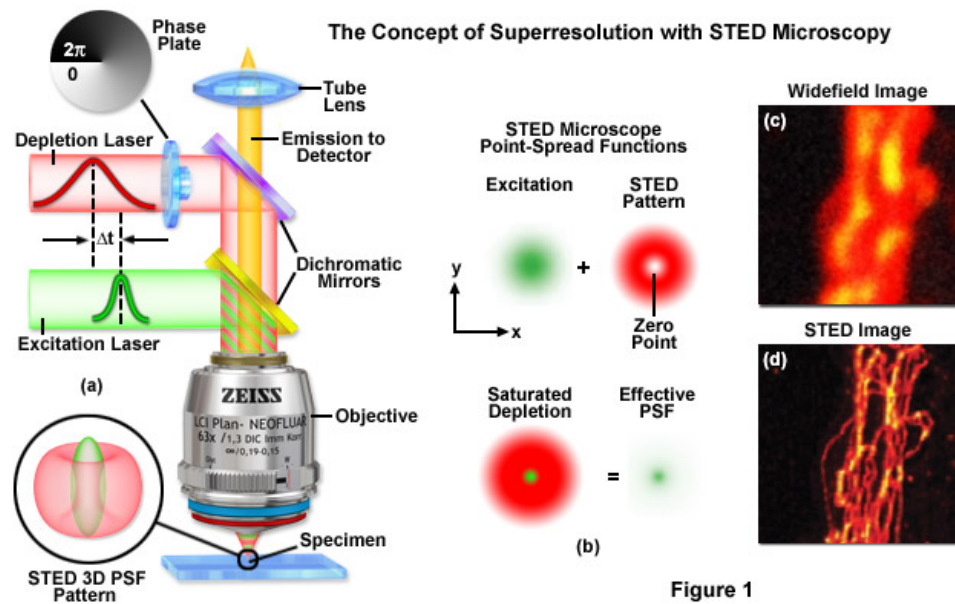
Figure 10. STED microscope setup and resulting effective fluorescence emission. A STED microscope uses two lasers of different wavelengths (excitation and depletion lasers) to reduce the excess fluorescence surrounding the point-spread function. This allows for increase resolution far beyond widefield microscopy.

STED super-resolution microscopy is a revolutionary microscopy technique, which is also very complex and challenging. When imaging beyond the diffraction limit, external forces such as vibration and spherical aberration have a larger impact. Biological samples are more easily photobleached by the intense quenching beam. Super-resolution imaging of such small structures also creates more noise in acquired images (Ulbirch, 2016).

1.4 Drosophila melanogaster as a model organism

Drosophila melanogaster, commonly known as the fruit fly, is a very well-understood model organism, easy and inexpensive to culture, and has a short life cycle. *Drosophila* are less genetically complex in comparison to humans,

containing only four chromosomes, and have fewer ethical impediments when used in biomedical research. Fruit flies are genetically orthologous to humans: 75% of human disease-causing genes have a recognizable match in the fruit fly, making it a good model organism for studying various diseases (Jennings, 2011).

1.4.1 *Drosophila* as model organism for studying the respiratory system

The mammalian respiratory organs, also known as lungs, are composed of a branched, tubular network that provides oxygen to different structures in the organism, but the underlying processes that control the development of this respiratory system are not well understood. The structures composing mammalian lungs are very complex, and, thus far, it has not been possible to completely map the genetic and cellular mechanisms that control their development (Ghabrial et al., 2003).

The *Drosophila* respiratory organ, otherwise known as the trachea, is also a tubular network that branches throughout the organism and provides oxygen to different structures in the *Drosophila* but has much simpler structure and genetics (Fig. 11). *Drosophila* have been proven as a reliable model system for studying various mechanisms underlying the process that dictates respiratory development, called tubular organogenesis. Tubular organogenesis in *Drosophila* is controlled by more than two hundred genes that compose several highly conserved signaling pathways. These signaling pathways orchestrate tasks within the *Drosophila*, such as cell specification, migration, and branch architecture (Loganathan et al., 2016).

Asthma and COPD (chronic obstructive pulmonary disease) are two of the most common inflammatory diseases of the mammalian airways, and over time, the prevalence of these diseases has continuously increased in western countries. These diseases have a very strong genetic component that has been identified in various inheritable asthma-susceptibility genes. *Drosophila* is an organism that shares a comparable organ composition and an equivalency to the mammalian lung, as well as an orthologous genetic model for studying the genes that lead to airway inflammatory diseases (Roeder et al, 2011).

Drosophila has proven to be advantageous as a model organism when compared to other commonly used model organisms, such as a transgenic mouse. Transgenic mice pose two problems: genetic redundancy and developmental plasticity. In the past, *Drosophila* have not been considered a useful model organism for studying airway inflammation due to their lack of an adaptive immune system. However, it has been discovered that many asthma-related genes are linked to innate immune responses and epithelial cell maintenance. Most asthma-related genes are expressed in the respiratory epithelium and are regulated upon infection in *Drosophila* (Roeder et al., 2008).
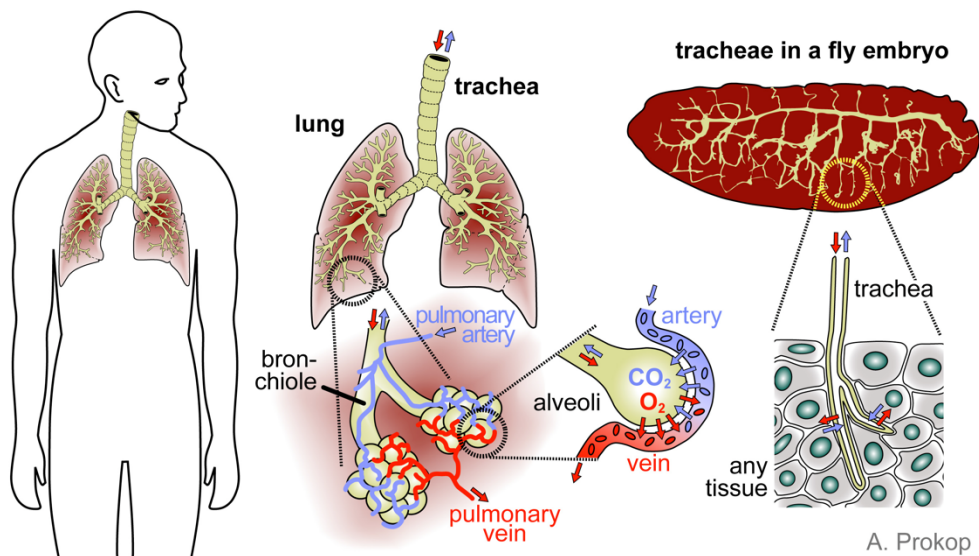
Figure 11. Schematic diagram of the parallels between human and *Drosophila* respiratory systems. Humans and flies both have an intricate branching system that allows oxygen and nutrients to be delivered to various organs and tissues within the organisms.

1.4.2 Development and anatomy of the *Drosophila* respiratory system

The *Drosophila melanogaster* respiratory system is composed of more than 10,000 interconnected tubes called trachea and terminal tracheoles that are made of a central lumen surrounded by an epithelial monolayer. The gas enters through spiracular openings on the *Drosophila* exoskeleton and travels through a sequential branching system of tubes until it reaches a tissue or organ. This sequential branching system follows a classification scheme: primary branch (also called the dorsal trunk), secondary branch, tertiary branch, etc. Primary and secondary branches are called trachea and all further branching is referred to as terminal branching or tracheoles. Structurally, the respiratory system has bilateral symmetry throughout the organism and a continual segmental organization

(Ghabrial et al., 2003). The trachea consists of a tracheal wall that contains a simple epithelial layer that includes the outermost, basement membrane of the wall. This epithelial layer functions as a barrier between the lumen and the sterile insides of the fly. Moving inward, the intima is composed of tubulin and chitin that forms ring-like structures called taenidia. Taenidia provide flexible integrity and structure to the trachea (Harrison, 2009) (Figure 12) (Ghabrial et al., 2003)(Weaver and Krasnow, 2008).
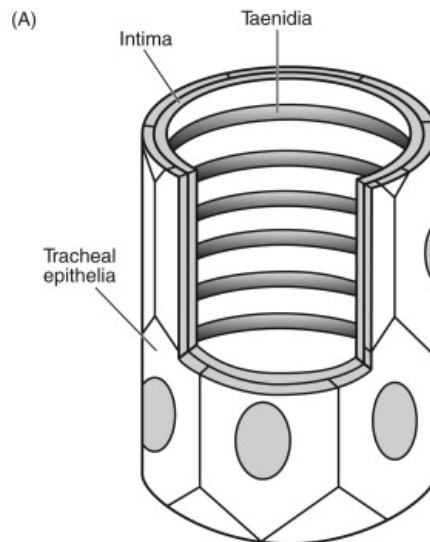
Figure 12. Schematic illustration of a *Drosophila melanogaster* trachea. The trachea is composed of taenidia that provides structure and an outer protective epithelial layer.

1.4.3 Tubulin and chitin provide structure to the *Drosophila melanogaster* taenidia

Tubulin is an abundant cytoplasmic, highly conserved protein that is found in all eukaryotes and exists as heterodimers of alpha and beta subunits. The alpha and beta tubulins form a dimer that is the building block of the microtubule. Tubulin polymerizes to form intracellular cylindrical filaments called microtubules (MTs). Microtubules are essential for several cellular processes, such as cell division and polarity, as well as intracellular transport, and must be well regulated due to its dynamic influence over free tubulin heterodimers (Baffet et al., add year). Tubulin is a structural protein that is a primary component of trachea. Tubulin function is regulated by the MT structure. MTs are fundamental components of the spindle in cell division, the axoneme in cilia and flagella, mediators of cell shape, and dynein/kinesin-based cell trafficking. All eukaryotes contain at least one major alpha (α1) and beta (β1) tubulin. In addition, *Drosophila*

melanogaster express minor, tissue-specific isoforms of tubulin in the motile spermtail axoneme (β2), pre-adult tissues (β3, β4, and α2), and the ovary (α4) (Nielsen et al., 2010).

Chitin is a structural polysaccharide made up of chains of modified glucose that is found in the cuticles of the exoskeleton of *Drosophila*. Chitin is also a primary component of the ring-like structures, called taenidia, that make up the tracheal system and the peritrophic matrices lining the epithelial tissue of the gut (Merzendorfer and Zimoch, 2003). During larvae development, the luminal accumulation of chitin provides the force for tube expansion (Hayashi and Kondo, 2018).

1.3 The NF-κB signaling pathway in fruit flies

The NF-κB (nuclear factor kappa B) pathway regulates the *Drosophila* immune system in response to infection, and incorrect regulation of this pathway is associated with increased inflammation and cellular proliferation (Taraborrelli and Walczak, 2015). NF-κB immune responses in *Drosophila* are regulated by two major pathways: the Toll pathway and the Imd pathway. The Toll pathway is activated upon infection by Gram positive bacteria and fungus causing the activation of NF-κB transcription factors Dorsal and DIF (Dorsal-related immunity factor). The Imd pathway is activated upon infection by Gram negative bacteria causing the cleavage of Relish, an NF-κB transcription factor (TF) (Hetru and Hoffmann, 2009). Ultimately, the NF-κB pathway transcription factor is released from inhibition and translocates into the nucleus from the cytoplasm, where it activates transcription of a plethora of genes, the main one being anti-microbial peptides (AMPs) (Figure 13). The NF-κB pathway is regulated by post-translational modifications (PTMs) and ubiquitination is one example of a PTM (Hetru and Hoffmann, 2009).
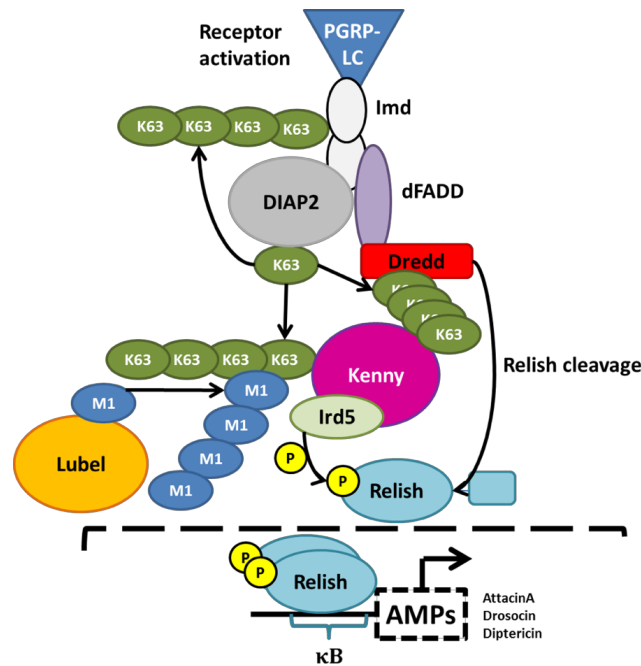
Figure 13. NF-κB Imd pathway in *Drosophila melanogaster*. The Imd receptor is activated upon infection by Gram negative bacteria causing the cleavage of the transcription factor, Relish. Relish is released from inhibition and translocates into the nucleus from the cytoplasm, where it activates transcription of anti-microbial peptides (AMPs). LUBEL catalyzes the formation of linear M1-linked ubiquitin chains on the K63 ligase, which ubiquitinates Kenny, (*Drosophila* IκB kinase γ), the regulator of the Imd pathway. LUBEL is required for the formation of M1-ub chains. Modified image from Anna Aalto.

1.3.1 Ubiquitination regulates the NF-κB pathway.

Ubiquitination is a post-translational modification that covalently binds ubiquitin moieties to target proteins and has been shown to regulate many biological processes. The ubiquitin protein is a highly conserved and dynamic protein which binds covalently to a lysine residue on the substrate. An isopeptide bond is formed between ubiquitin and the substrate in an enzymatic cascade involving three proteins: E1, E2 and E3. E1 is the ubiquitin-activating enzyme. E2 is the ubiquitin-conjugating enzyme. E3 is the ubiquitin-protein ligase. Ubiquitin itself contains seven lysine residues and an N-terminal methionine where ubiquitin moieties can bind via isopeptide linkages forming polyubiquitin chains. Depending on the lysine/methionine used for linkage, different types of ubiquitin chains are formed with different chain topologies (Swatek and Komander, 2016). The various chain conformations are recognized by UBD (ubiquitin D) containing proteins. For example, the proteasome lid recognizes K48-linked chains; therefore, K48 chains

are associated with protein degradation. The ubiquitination is a reversible modification. The ubiquitin chains can be removed by deubiquitinates (DUBs) such as CYLD, which removes methionine 1-ubiquitin chains from Kenny in the Imd pathway, thus reversing the ubiquitination (Aalto et al.,2019).

1.3.2 M1-linked ubiquitination in *Drosophila melanogaster*

LUBEL is an E3 ligase that specifically catalyzes the formation of M1 (methionine 1)-linked linear ubiquitin chains in *Drosophila*. LUBEL is orthologous to mammalian HOIP (HOIL-1-interacting protein) (Figure 14). HOIP is a part of the M1- linear ubiquitin chain assembly complex (LUBAC), which is important for NF-κB pathway regulation and subsequently, inflammatory signaling in humans (Spit et al., 2019). Similarly, linear ubiquitin chains are important for the activation of regulatory pathways in *Drosophila*, such as the NF-κB pathway. (Aalto et al., 2019). It has been shown that LUBEL catalyzes the formation of M1-linked ubiquitin chains, which targets Kenny (*Drosophila* IκB kinase γ), the regulator of the Imd pathway. Ubiquitination of Kenny is necessary for the activation of Relish, which then translocates into the nucleus and can activate AMP (antimicrobial peptide) gene expression, which elicits an inflammatory response in the fly (Aalto et al., 2019)
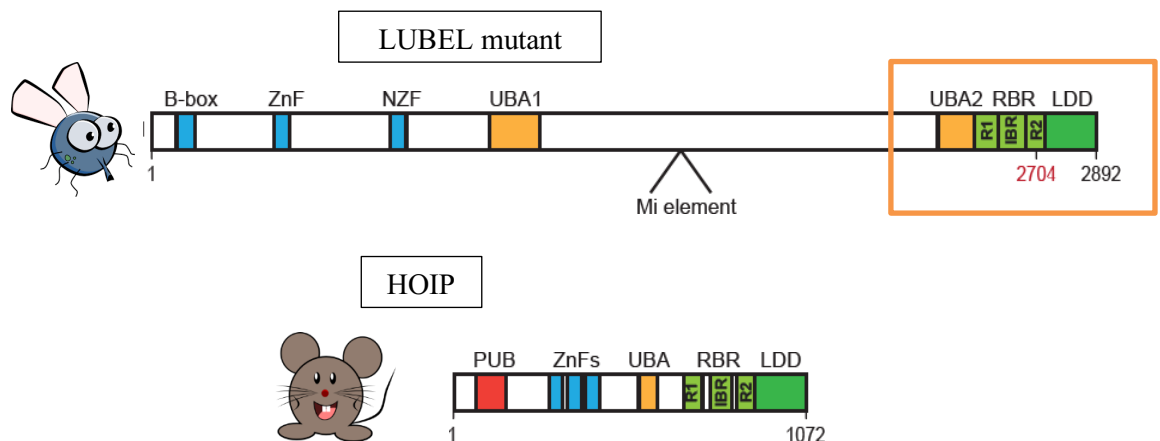

Figure 14. HOIP (HOIL-1-interacting protein) is the mammalian orthologue of *Drosophila* LUBEL (linear ubiquitin E3 ligase). LUBEL mutant is formed when a transposable minos element is inserted into the gene, there is a loss of function in LUBEL due to the inactivation of the RBR catalytic domain.

1.6 HIF pathway in Drosophila

The HIF (Hypoxia Inducible Factor) pathway is a hypoxia-induced signaling pathway that stabilizes the *Drosophila* HIF-α Sima protein and translocates it into the nucleus for targeted gene expression in low oxygen conditions. In normoxic conditions, Sima is constantly being produced, but as long as there is oxygen in the system, it is hydroxylated by oxygen-sensing PHDs (prolyl-hydroxylases) on the oxygen-dependent degradation domain (ODD) of the HIF-α Sima. Hydroxylated Sima is recognized by the K48-ubiquitin E3-ligase complex and targeted for proteasomal degradation (Figure 15). It has been defined in previous literature that NF-κB plays a role in cellular response to hypoxia, but the exact molecular mechanics are unknown (D'Ignazio and Rocha, 2016).
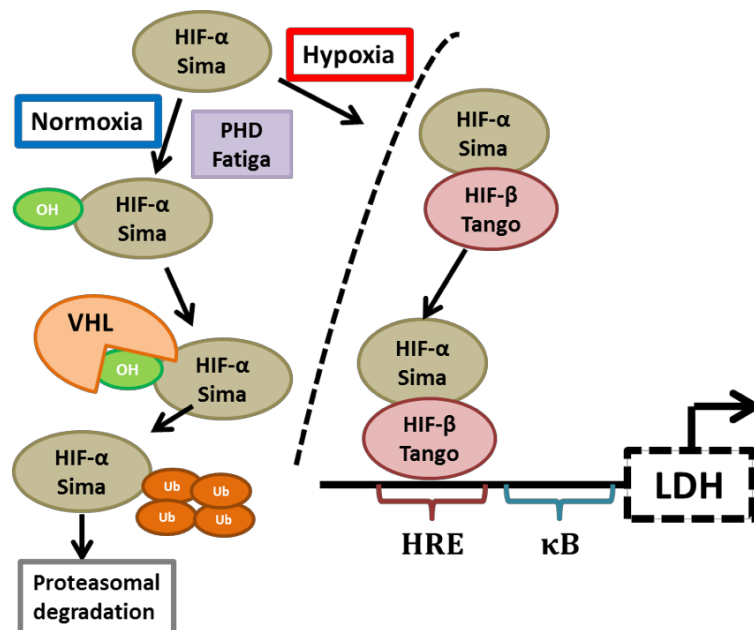
Figure 15. HIF signaling pathway in *Drosophila melanogaster*. In normoxic conditions, Sima is constantly being produced, but as long as there is oxygen in the system, it is hydroxylated by oxygen-sensing PHDs (prolyl-hydroxylases) on the oxygen-dependent degradation domain (ODD) of the HIF-α Sima. Hydroxylated Sima is recognized by the K48- ubiquitin E3-ligase complex and targeted for proteasomal degradation. Where there is a lack of oxygen, the pathway is sent into hypoxia and the HIF-alpha sima conjugates to HIF-beta tango and transcribes LDH (lactate dehydrogenase).

1.6.1 M1-linked ubiquitination in hypoxia

The role of ubiquitination and especially the role of K48-linked ubiquitination has been extensively studied in the hypoxia response signaling, however the role of M1-linked linear ubiquitination has not been previously studied in *Drosophila*. Preliminary results from our lab show that M1-linked ubiquitin chain formation is

induced upon hypoxia, When further analyzing the role of M1-linked ubiquitination in hypoxic conditions, with the help of LUBEL mutant flies, it was discovered that LUBEL mutant flies are unable to form M1- linked ubiquitin chains and die in hypoxic conditions, whereas wild-type *Canton^s* flies survive (Figure 16) (unpublished).

.

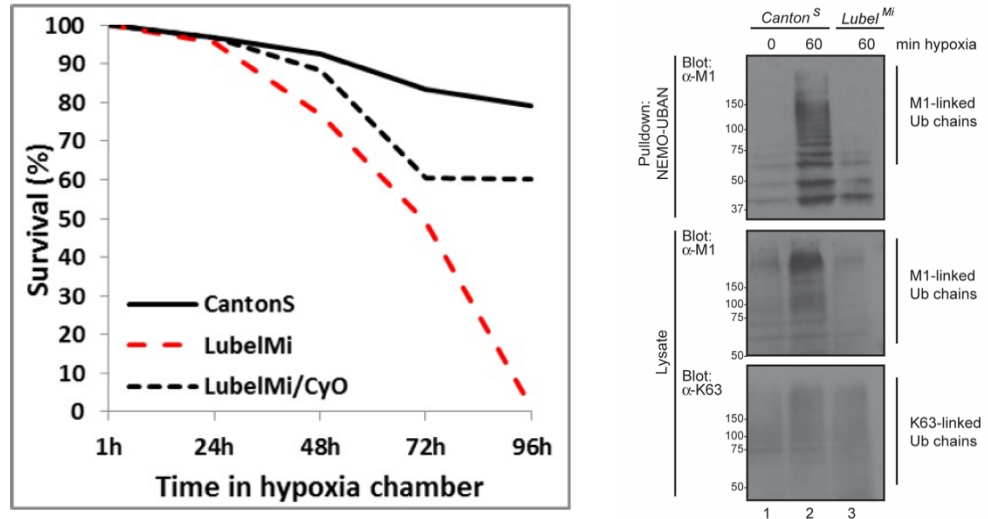Figure 16. Homozygous *lubel^Mi* flies die in hypoxic conditions in comparison to wild-type *Canton^S* flies (left). M1-linked ub chains decreased in LUBEL mutant flies in hypoxia in comparison to wild-type flies.

2. AIMS AND HYPOTHESIS

According to previous scientific literature and preliminary lab results, I present the following hypotheses and aims to understand the role of LUBEL in the *Drosophila* respiratory system:

2.1 Hypothesis 1: The tracheal epithelial tissue is malformed in LUBEL mutant flies lines.

It has been shown that the overexpression of the RBR-catalytic domain in gut tissue of *lubel^{Mi}* flies causes hyperproliferation, and a lack of LUBEL causes a lack of response to infection. Both the trachea and gut are composed of simple epithelial tissue (Aalto et al., 2019). We hypothesize that the mutant flies have a similar response in the tracheal epithelial tissue, which causes malformed morphology and asphyxiation.

Aim 1: Investigate *Drosophila* tracheal epithelial tissue in wild type and LUBEL mutant flies. To investigate hypothesis 1, I aim to characterize wild-type fly tracheal morphology (diameter, thickness, taenidia appearance) and establish a trachea dissection and staining protocol for third instar larvae. Lastly, compare tracheal morphology in *Canton^S* and *l* LUBEL mutant larvae.

2.2 Hypothesis 2: The hypoxia response signaling pathway is not functional in lubel^{Mi} flies.

We hypothesize that LUBEL is interfering with Sima signaling; therefore, the mutant flies experience a disruption in the hypoxia-induced signaling in the absence of LUBEL. This interruption in hypoxia-induced signaling will compromise the hypoxia response in the flies, making them sensitive to low-oxygen conditions.

Aim 2: Investigate HIF-signaling in *Canton^s* and *lubel^Mi* flies

To study HIF signaling error, I will conduct live larvae imaging of *GFP-ODD* flies, where the ODD domain of HIF1-alpha is conjugated to the green fluorescent protein (GFP). Under normal oxygen conditions the ODD domain of fly HIF1-a Sima is targeted for proteasomal degradation, however upon hypoxia, the ODD is stabilized. In this way HIF signaling activity can be monitored with the help of the conjugated GFP. The GFP-ODD flies crossed with LUBEL mutant flies can be used to monitor the role of M1-linked ubiquitination in activation of the HIF signaling pathway. Also, the GFP-ODD flies can be used in normoxic and hypoxic condition and compare tracheal branching in *Canton^s* and *lubel^Mi* larvae.

With these two projects aims I will further elucidate on the question why LUBEL mutant flies succumb in low-oxygen conditions. In this thesis, I will only present results from aim 1. The GFP expression and fluorescent signal of the GFP-ODD flies could not be detected in flies even after innumerous optimization steps.

3. MATERIAL AND METHODS

Drosophila fly lines:

Canton^S: control fly line

DaGal4: control fly line

lubel^{Mi}: LUBEL mutant fly line with a transposable Minos element inserted in the gene before the catalytic RBR domain that is unable to form M1-linked ubiquitin chains

lubelRNAi: LUBEL mutant fly line due to RNA interference

GFP-ODD: transgenic fly line expressing GFP tagged on the oxygen-dependent degradation domain of the HIF-alpha Sima

Fly husbandry

Drosophila melanogaster were maintained at 25 °C with a 12 h light–dark cycle on Nutri-fly BF (Dutscher Scientific). *Canton*^{S} wild-type flies, *DaGal4* driver lines, *DaGal4, Dipt- LacZ* reporter lines, and balancer lines, as well as dreddL23 and spätzleRM7 mutant flies were kindly provided by Prof. Pascal Meier [60, The *Drosophila* fly lines w:RelE20 (stock #9457), yw;Mi{ET1}LUBELMB00197 (stock #22725 referred to as *lubel*^{Mi}) and Mi{MIC}LUBELMI14859 (stock #59639 referred to as 1 *lubel*^{MiMic}) were obtained from Bloomington stock center.

***Drosophila* dissections and fluorescent staining**

Third instar larvae are dissected in order to optimize tracheal imaging. The larvae are placed in -20 °C for approximately 30 minutes before dissection in order to immobilize them. Then the larvae are carefully opened with micro scissors, pinned on gel dissection plates, and all internal structures are removed, leaving behind only the tracheal system and the exoskeleton (Figure 17) (dissection protocol according to Feng Chen bio-protocol "Preparation and Immunofluorescence Staining of the Trachea in *Drosophila* larvae and pupae).
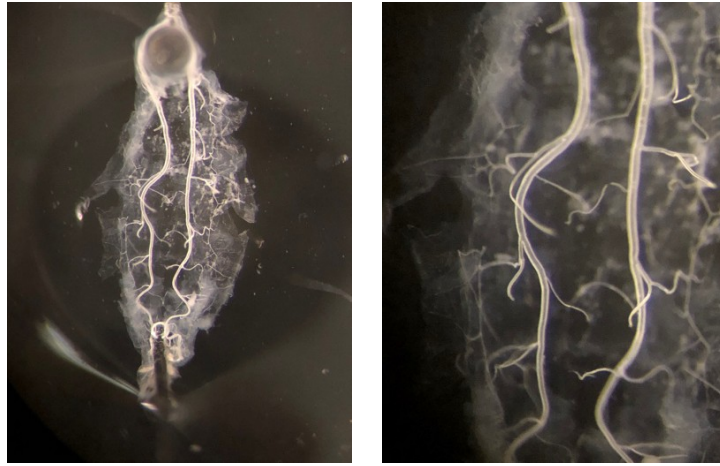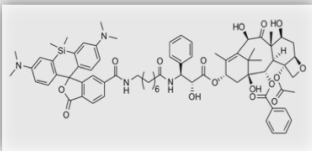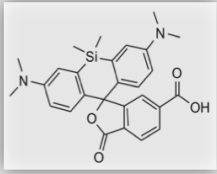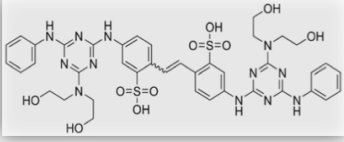
Figure 17. Dissected *lubel*^{Mi} third instar larvae featuring only the respiratory system and exoskeleton.

After dissections, the larvae are placed in PBS in a 24-well plate (pre-coated with 1 % BSA-PBS to reduce stickiness of well plastics). Then the larvae are stained with a specified fluorophore according to the structure of interest (Table 1). For full optimized staining protocol see Appendix 1, in short:

Once the larvae are dissected and prepared for staining, remove the PBS from each well and add 250 μL of staining solution: 1 μM SiR-Tubulin/SiR-COOH, 1 μM Verapamil, and 1 μM Calcofluor White in 1xPBS. Incubate the larvae for 1.5 hour in the dark at room temperature. Before mounting samples on microscope slide quickly rinse of staining solution with PBS. When mounting the samples, place two spacers (double-sided tape) on the microscope slide and apply 5 μL of Moviol mounting media in between the spacers. Then position the larvae with the trachea facing upwards on the microscope slide. On a clean cover glass, place ~4 μL of Moviol and place the cover glass over the sample.

Table 1: Chitin-specific and tubulin-specific silicone rhodamine (SiR) probes and Calcofluor White staining

Molecule	Fluorophore	Excitation/Emission	Microscope	Target
	SiR-Tubulin SiR and the microtubule binding drug Docetaxel	652/674	• Zeiss LSM880 with AiryScan • Abberior STED	*Drosophila* larvae respiratory tubulin
	SiR-COOH 6-carboxylic acid form of SiR dyes as markers for chitin	652/674	• Zeiss LSM880 with AiryScan • Abberior STED	*Drosophila* larvae chitin-containing taenidia, a component of tracheoles
	Calcofluor White Stain non-specific fluorophore that binds to cellulose and chitin	355/300-440	• Zeiss LSM880 with AiryScan • Zeiss Axio Vert.A1	*Drosophila* larvae taenidia

Imaging acquisition using Zeiss LSM880:

Imaging using desired magnification at the microscope (40x is useful for identifying ROI). In the Zeiss interface, image using the "Smart Setup" for Cy5, Calcofluor white, and FITC channels. Choose the option for "best signal" and use separate tracks for highest signal intensity. Acquire the images using optimal frame size unless otherwise justified, acquisition speed 6-8 and averaging in line mode. Adjust the laser power to 2-5%, gain to ~800, and offset from zero to -10 or higher. Always set pinhole to 1 airy unit unless otherwise justified.

Image processing in Fiji:

Acquired images were processed using ImageJ. The images were acquired as Z-stacks and the Z-stacks were compiled into a single image using the Z-projection feature in Fiji. The maximum intensity or average intensity projection was used depending on image saturation levels. Linear adjustments were made as needed to brightness and contrast (adjust maximum and minimum values to highlight target features in your images). When taking dorsal trunk measures, use the drawing tool to draw a straight line from one end of the dorsal trunk to the other. Record the measurement of the line as dorsal trunk width in microns.

Tracheal diameter measurements and statistical analyses

Three different measurements were taken from brightfield images of the dorsal trunks of dissected third instar larvae. From all four fly lines the average dorsal trunk width was calculated. Results from the measurements were analyzed by one-way analysis of variance (ANOVA), with Tukey's multiple comparison posttest for 95% confidence interval. In figures, ns stands for $p > 0.05$, * for $p < 0.05$, ** for $p < 0.01$, *** for $p < 0.001$ and **** for $p < 0.0001$. Error bars in figures specify SEM from the indicated number of independent experiments. The measurements were done in three experimental repeats using at least three flies per repeat.

4. RESULTS

4.1 Optimization of staining protocol for visualizing trachea in wild-type fly line.

4.1.1 Optimization of SiR-tubulin and SiR-COOH staining protocols in Drosophila.

Newly developed silicone rhodamine (SiR) organic fluorophores have been shown to be a highly permeable and photostable staining technique for imaging *Drosophila* microtubules and tracheoles in dissected tissues (Lukinavičius et al., 2018). In order to utilize this organic fluorophore for imaging the airways in *Drosophila* third instar larvae, a novel staining protocol was developed and optimized for the purpose of my research using two specific SiR fluorophores: SiR-tubulin and SiR-COOH (Fig. 18). Upon initial staining attempts using 1 µM SiR-tubulin and 1 µM SiR-COOH, SiR-tubulin staining in dissected *Canton^S* larvae showed specific staining with low background noise when imaged using Zeiss LSM880 confocal microscope (Fig. 18A). SiR-COOH, which targets chitin structures within the taenidia of the airways, stained with less specificity and unevenly throughout the sample (Fig. 18B).

After a series of trial and error and various optimizations to the novel staining and dissection protocol, there was an improvement in the SiR-tubulin staining specificity and intensity when the samples were incubated for a longer period of time (~1.5 hour) in a smaller volume of staining solution (250 µL) (Fig. 18C). SiR-COOH staining did not show such improvement in the specificity or intensity after these optimizations were applied to the protocol. The structure of the dissected *Drosophila* trachea can be clearly seen, but there is still an abundance of unspecific background staining (Fig. 18D). Due to this, SiR-COOH staining techniques were no longer used for the remainder of the project because the lack of specificity in the staining did not suit the needs of the project.
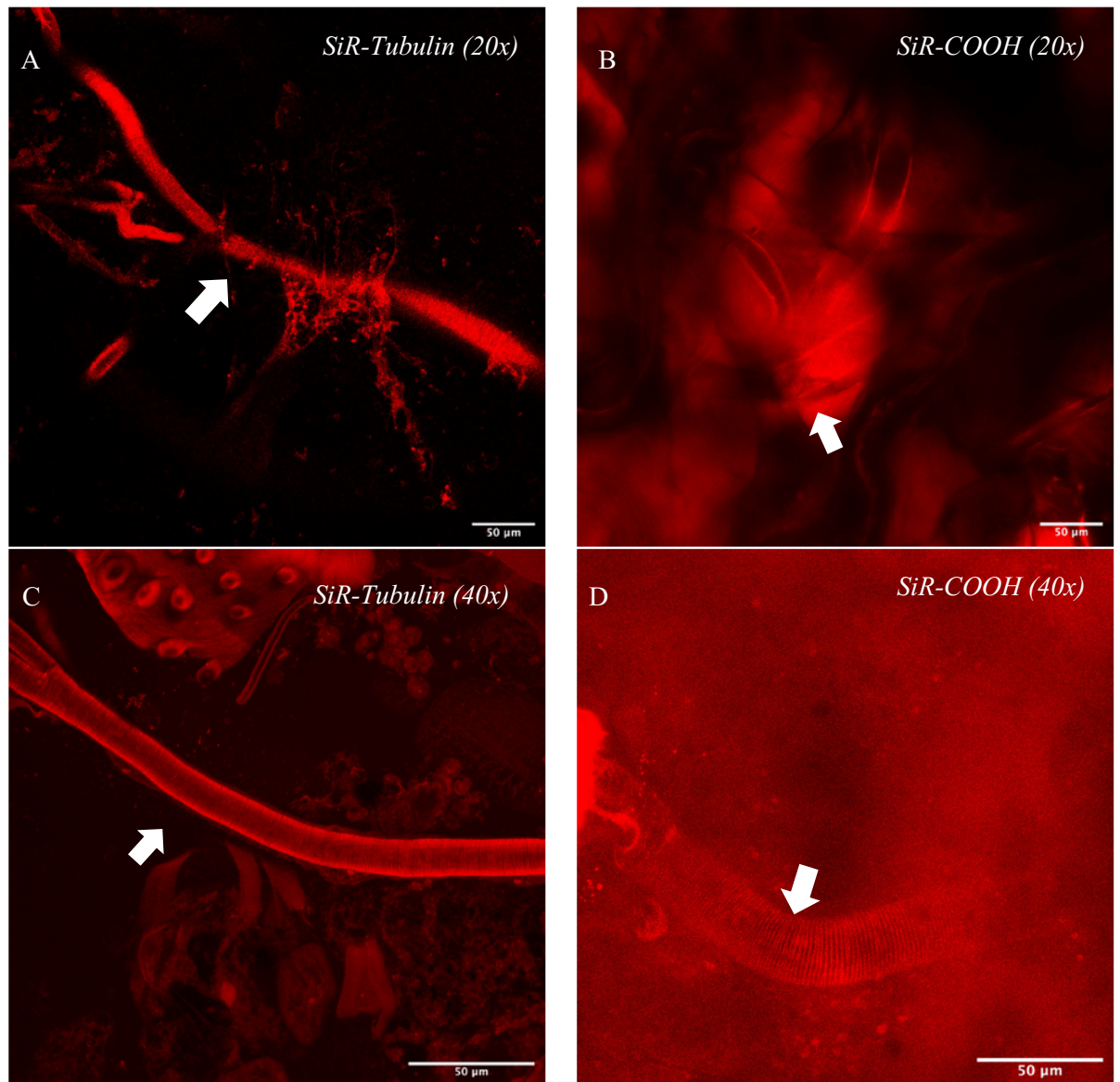
Figure 18. Dissected trachea from *Canton^S* third instar larvae stained with various SiR probes and imaged using Zeiss LSM880. **a-b** Representative images of the dorsal trunks (indicated with arrows) stained using a pre-optimized dissection and staining protocol (**a**) 1 µM SiR-Tubulin (20x) (**b**) 1 µM SiR-COOH (20x). **c-d** Representative images of the dorsal trunks stained using the SiR staining and dissection protocol post-optimizations (**c**) 1 µM SiR-Tubulin (40x) (**d**) 1 µM SiR-COOH (40x). Scale bars: 50 µm. All images were processed and analyzed using MIP and LUT red in Fiji.

4.1.2. Calcofluor white staining in Drosophila highlights chitin structures.

Calcofluor White stain by Sigma-Aldrich is a reputible, non-specific fluorophore that binds to cellucose and chitin in cell walls. It successfully and specifically stains the chitin-composed taenidia in the dorsal trunk of *Drosophila*, as well as the exoskeleton. Due to the ease and consistency of this staining technique, Calcofluor white staining was used in place of SiR-COOH staining to visualize the ring-like taenidia in the *Drosophila* airways (Fig. 19).
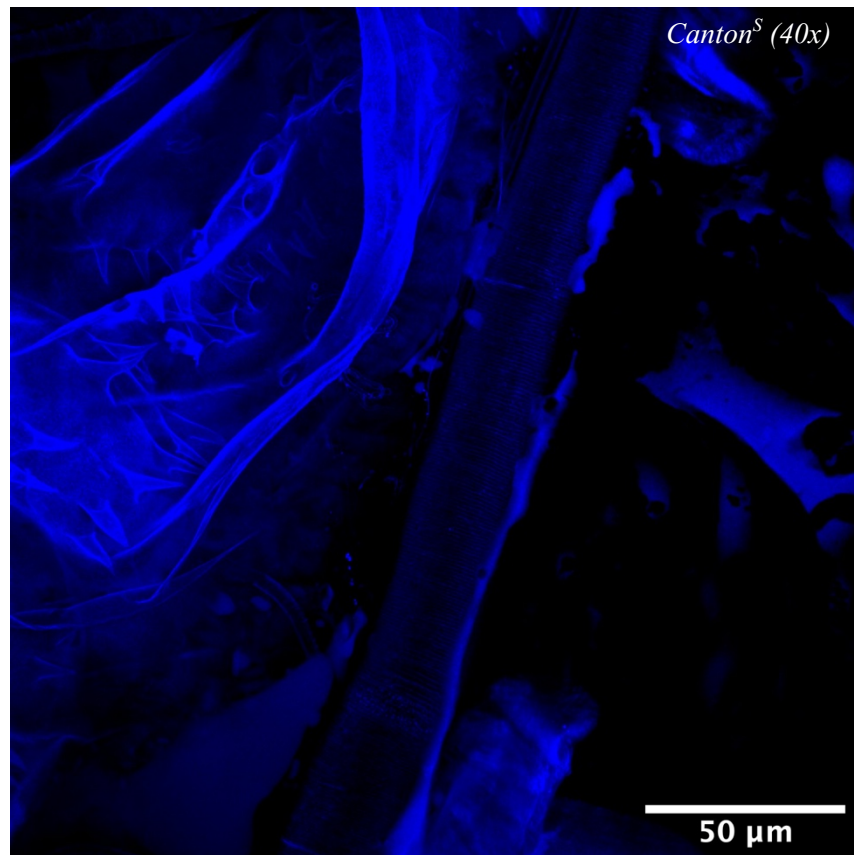

Figure 19. Dissected trachea from *Canton^S* third instar larvae stained with 1 µM Calcofluor White 18909 and imaged using Zeiss LSM880. The chitin structures in the dorsal trunk and in the exoskeleton are emphasized. Scale bar: 50 µm. The image was processed and analyzed using MIP and LUT blue in Fiji.

4.2 Loss of LUBEL causes malformed epithelial morphology in Drosophila trachea.

In order to investigate any change in morphology of the respiratory system in *Drosphophila* third instar larvae upon removal of LUBEL, a baseline morphology was established for wild-type *Drosophila.* Wild-type *Canton^S* larvae were stained with 1 µM SiR-tubulin and imaged using Zeiss LSM880. The airways of wild-type *Drosophila* larvae have periodic, ring-like taenidia that have a uniform pattern across the entire length of the dorsal trunk surface in basal conditions (Fig. 20A). Upon removal of LUBEL, there is a change in the morphology of the dorsal trunk surface. Mutant *lubel^{RNAi}* and *lubel^{Mi}* larvae were stained with 1 µM SiR-tubulin and imaged using Zeiss LSM880 (Fig. 20B-C). The taenidia of the dorsal trunk in the mutant fly lines have abnormal finger-like structures that project from the surface of the respiratory tube. This is a morphological feature that was only seen in fly lines that lacked LUBEL.
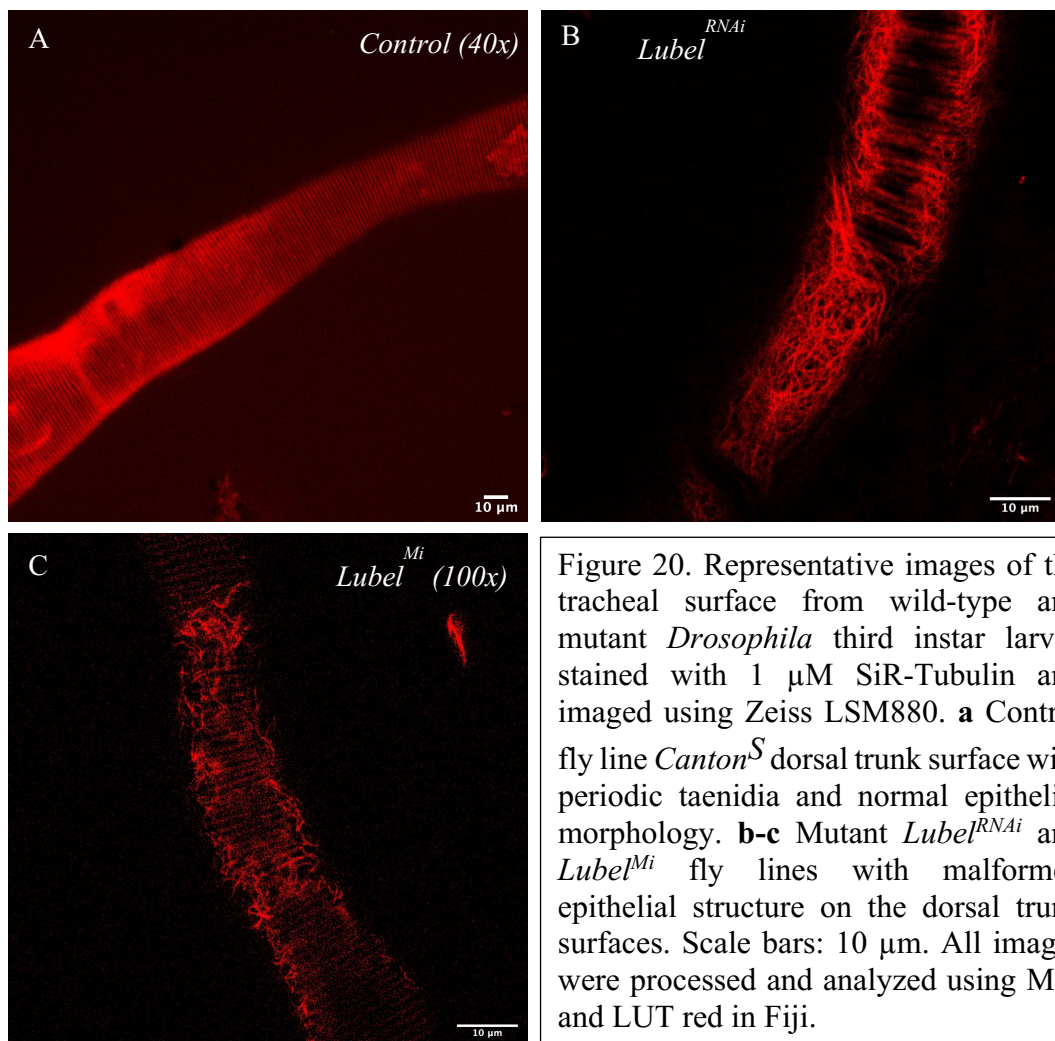
Figure 20. Representative images of the tracheal surface from wild-type and mutant *Drosophila* third instar larvae stained with 1 µM SiR-Tubulin and imaged using Zeiss LSM880. **a** Control fly line *Canton^S* dorsal trunk surface with periodic taenidia and normal epithelial morphology. **b-c** Mutant *Lubel^{RNAi}* and *Lubel^{Mi}* fly lines with malformed epithelial structure on the dorsal trunk surfaces. Scale bars: 10 µm. All images were processed and analyzed using MIP and LUT red in Fiji.

4.3 STED imaging of the malformed epithelial morphology in small-order tracheal branching in Drosophila.

After seeing the presence of this abnormal epithelial morphology on the surface of the dorsal trunk in mutant fly lines, I used SiR-tubulin and STED imaging to investiage the smaller-order branches in wild-type and LUBEL mutant fly lines to determine if this abnormal phenotype existed only on the dorsal trunk of the larvae or on the smaller structures as well. In order to establish a baseline morphology for smaller-order branching in wild-type *Drosophila, Canton*^{S} larvae were stained with 1 µM SiR-tubulin and imaged using the Abberior STED 775 Quad scanning microscope. As seen on the surface of the dorsal trunk, smaller, fifth-order tracheoles in wild-type larvae also exhibited periodic, ring-like taenidia with a uniform pattern (Fig. 21A).

Upon removal of LUBEL, there is abnormal epithelial morphology of the tracheole surface in smaller respiratory structures. Mutant *lubel*^{Mi} larvae were stained with 1 µM SiR-tubulin and imaged using the Abberior STED 775 Quad scanning microscope (Fig. 21B). The taenidia of the smaller, fourth-order tracheoles in the mutant fly line have abnormal finger-like structures that project from the surface of the respiratory tube, as seen on the larger dorsal trunk. These abnormal projections are not continuous on the entirety of the respiratory tube (Fig. 21C-D). This is a morphological feature that was only seen in fly lines that lacked and could be seen in various order of branching.

Control (100x) Confocal

STED 5 µm
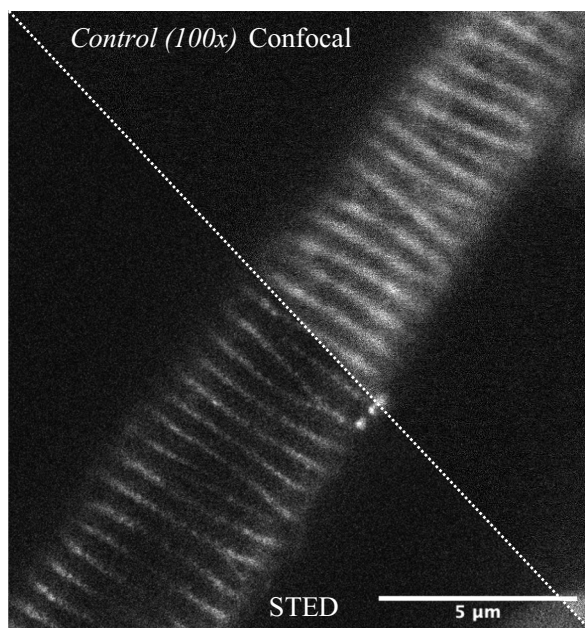
Figure 21a Confocal and STED image of fifth-order tracheoles from *Canton*^{S} third instar larvae stained with 1 µM SiR-Tubulin and imaged using Abberior STED 775 Quad. Taenidia epithelial structures are periodic in wild-type larvae. Scale bar: 5 µm. All images were processed and analyzed in Fiji.
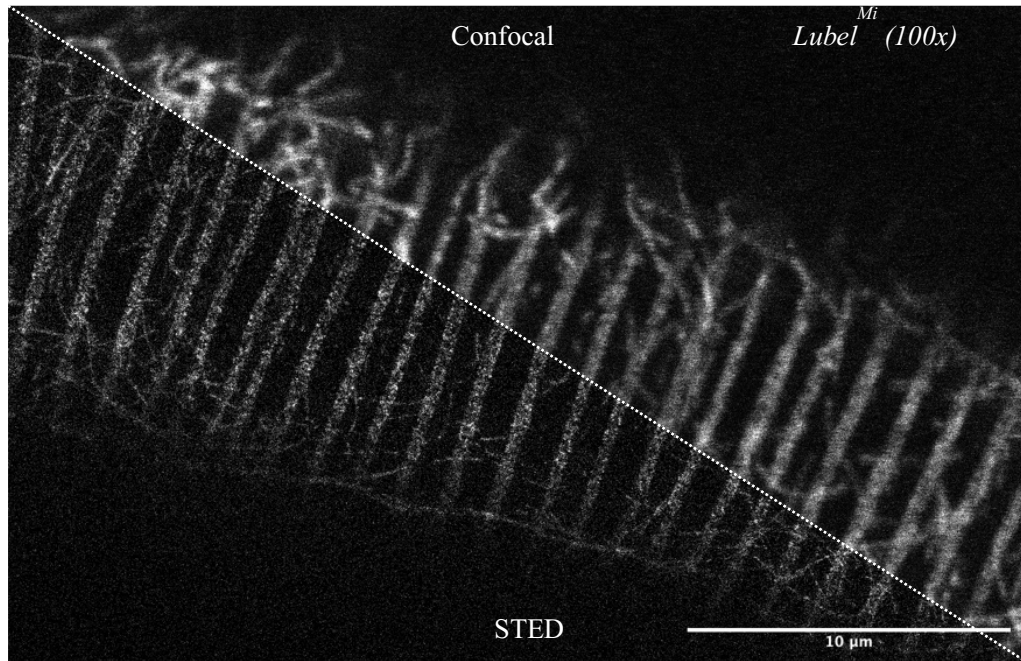
Figure 21B. Confocal and STED image of fourth-order tracheoles from *Lubel*^{Mi} third instar larvae stained with 1 µM SiR-tubulin and imaged using Abberior STED 775 Quad. Taenidia epithelial structures are irregular in LUBEL mutant larvae. Scale bar: 10 µm. All images were processed and analyzed in Fiji.
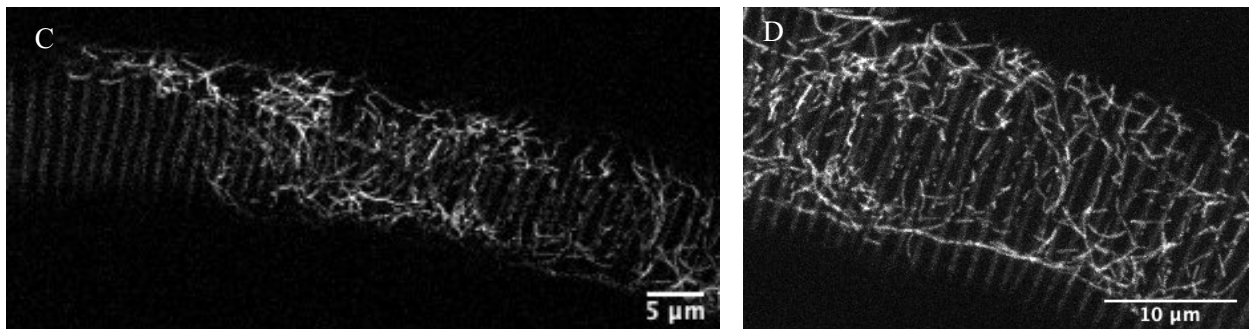
Figure 21C-D. STED image of fourth-order tracheoles from *Lubel*^{Mi} third instar larvae stained with 1 µM SiR-Tubulin and imaged using Abberior STED 775 Quad. **C** Taenidia epithelial structures are irregular in LUBEL mutant larvae, and this irregularity is not constant across the entire tracheole. Scale bar: 5 µm. **D** Abnormal finger-like structures clearly project from the surface of the respiratory tube. Scale bar: 10 µm. All images were processed and analyzed in Fiji.

4.4 Quantitative analysis of dorsal trunk thickness in Drosophila third instar larvae.

After several experimental repeats, I also noticed that the dorsal trunks in LUBEL mutant fly lines appeared wider than the wild-type fly line, in addition to the abnormal epithelial morphology in LUBEL mutant larvae. To test this observation, I measured the average dorsal trunk width in four different fly lines: *Canton^S* (control 1), *DaGal* (control 2), *lubel^{Mi}* (LUBEL mutant 1), *lubel^{RNAi}* (LUBEL mutant 2). Three different measurements were taken from brightfield images of the dorsal trunks of dissected third instar larvae, as shown in Fig 4A, from all four fly lines and the average dorsal trunk width was calculated. This was done in three experimental repeats using at least three flies per repeat. In both mutant fly lines (*lubel^{Mi}* and *lubel^{RNAi}*), there was a significant increase in average dorsal trunk width in comparison to both control groups (Fig. 22B-C).

Additionally, Tukey's multiple comparison test shows that there is no significant difference in the average dorsal trunk width between the two control groups, further verifying *DaGal* as a suitable control group. Also, there is no significant difference between the two mutant groups, which suggests that the increased average dorsal trunk width in LUBEL mutant fly lines is independent of the method used to silence LUBEL in the fly (Fig. 22C). The increase in average dorsal trunk width in the two mutant fly lines in comparison to the control fly lines shows that there is a quantifiable change in the morphology in the absence of LUBEL.

C
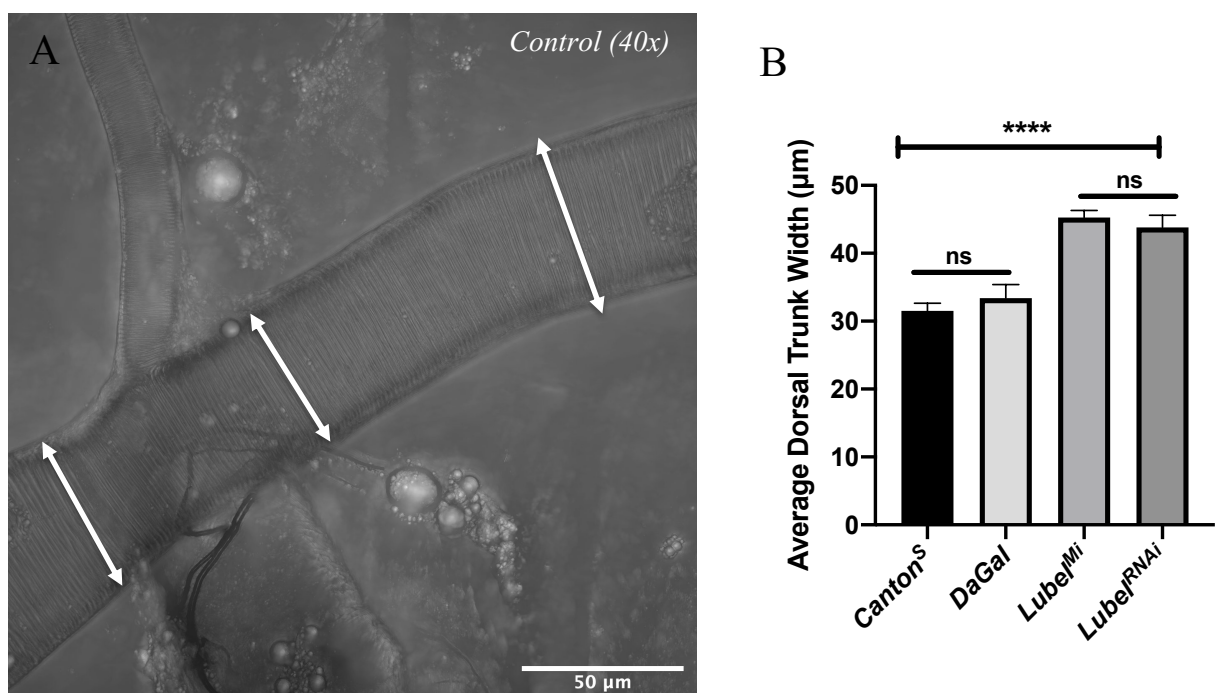
Tukey's multiple comparisons test	Mean Diff.	95.00% CI of diff.	Significant?	Summary
$Canton^S$ vs. $Lubel^{Mi}$	-13.73	-19.46 to -7.991	Yes	****
$Canton^S$ vs. $Lubel^{RNAi}$	-12.26	-18.00 to -6.526	Yes	****
$Canton^S$ vs. $DaGal$	-1.866	-7.602 to 3.869	No	ns
$Lubel^{Mi}$ vs. $Lubel^{RNAi}$	1.466	-4.270 to 7.201	No	ns

Figure 22. Larvae with mutated LUBEL have increased dorsal trunk width.
a Representative image of a wild-type $Canton^S$ larvae that were dissected and imaged using Zeiss LSM880 brightfield microscopy. Using a Z-stack, the average dorsal trunk width was calculated using three different measurement points (indicated with arrows). **b** Larvae wild-type $Canton^S$, control $DaGal$, $Lubel^{Mi}$ mutant, and $Lubel^{RNAi}$ mutant flies were dissected and imaged using Zeiss LSM880 brightfield microscopy. The average dorsal trunk width was calculated using three different measurement points from three experimental repeats using at least three flies per repeat. Error bars indicate standard error of mean. **c** Tukey's multiple comparison test from the one-way ANOVA shows that there is no significant difference in the average dorsal trunk width between the two control groups ($Canton^S$ vs $DaGal$), while there is a significant difference between the average dorsal trunk width in each control group in comparison to each mutant groups.

5. DISCUSSION

5.1 Staining of the taenidia in Drosophila melanogaster larvae

In order to analyze the morphology of the respiratory system in *Drosophila melanogaster* larvae, I targeted two primary, structural components of the tracheal system: tubulin and chitin. Throughout the course of this project, SiR-tubulin has proven to be an effective and useful staining method for examining the respiratory system of *Drosophila* larvae (Figure 1 results). When paired with the Zeiss LSM880 scanning confocal microscope, one is able to obtain clear, detailed images of the larvae dorsal trunk and smaller tracheoles. SiR-COOH, which stains specifically for chitin, a structural component of larval taenidia, over-saturated the samples which made distinguishing finer structures in the tracheoles very difficult. Due to time restraints surrounding the project, I did not spend additional time further optimizing the SiR-COOH staining, but instead used Calcofluor White, which has been proven in other literature to be an easy and simple chitin-specific staining.

The unspecific background staining using SiR-COOH could be caused by the high amounts of chitin in *Drosophila* exoskeleton (Zimoch et al, 2005). When dissecting the samples, all other internal structures were removed from the larvae excluding the dorsal trunks and tracheole network that is connected to the exoskeleton (reference image of dissected larvae). The high saturation levels seen in SiR-COOH stained samples were not seen in Calcofluor white stained samples. Although both dyes are chitin specific, Calcofluor white is activated by UV excitation light, which has a shorter wavelength in comparison to IR light that activates SiR probes. This shorter wavelength restricts the imaging depth of the sample, which could contribute to the lower signal intensity of Calcofluor white stained samples. With further optimizations steps, such as testing different staining concentrations, incubation times, and washing techniques, SiR-COOH could be a potentially useful staining technique for imaging *Drosophila melanogaster* taenidia, with special consideration of STED imaging. STED imaging requires far-red excited probes.

When considering future experiments in the lab, it would be desirable to image the tubulin in LUBEL-mutant flies using other types of tubulin and chitin staining techniques. Immunostaining using a primary and secondary antibody is a very well-established and traditional staining method and could be good to validate the results from the SiR staining.

5.2 LUBEL-mutant larvae express novel, phenotypic abnormalities in the respiratory system.

5.2.1 *lubel^{RNAi}* and *lubel^{Mi}* have abnormal tubulin structures on the dorsal trunk and tracheoles.

Larvae that lack LUBEL (*lubel^{RNAi}* and *lubel^{Mi})* express a phenotype I have described as "abnormal, finger-like tubulin projections" from the surface of the dorsal trunk as well as smaller tracheoles. This is a phenotype that I did not expect to see, but after several experimental repeats using *lubel^{Mi}* and *Canton^S* larvae, I observed finger-like projections from the surface of the dorsal trunk in random *lubel^{Mi}* larvae, but I did not see this phenotype in wild-type *Canton^S* larvae. To investigate whether or not these finger-like structures were due to malformed tubulin or chitin, I stained the samples using SiR-tubulin and Calcofluor white and looked at these probes under different channels. The abnormal phenotype could be seen under the Cy5 red channel that excited SiR probes, but not under the UV channel that excites Calcofluor white probes; therefore, this is an indication that the abnormal phenotype is tubulin specific.

To determine whether or not this phenotype was due to a lack of LUBEL or just a special phenotype in *lubel^{Mi}* flies, a second mutant was added to the experimental setup. *lubel^{RNAi}*, which is a LUBEL-mutant fly line that does not express LUBEL due to RNA interference, versus a lack of LUBEL by removing the RBR catalytic domain as in *lubel^{Mi}* flies. This abnormal tubulin phenotype was seen in both *lubel^{RNAi}* and *lubel^{Mi}* fly lines, validating that it is due to a lack of LUBEL. Additionally, to verify that the abnormal tubulin structure was not merely a phenotype that was lacking in *Canton^S* flies, a second control group was added, *DaGal* fly line. *DaGal, daughterless-GAL4* driver fly line, did not express the abnormal tubulin phenotype, which further validates that the abnormal tubulin phenotype is only in flies with mutated LUBEL.

For future experiments, additional LUBEL mutant fly lines could be imaged using SiR-tubulin as well as other methods of tubulin staining to further validate that it is due to a lack of LUBEL. Also, to further study the role of LUBEL, the RBR-catalytic domain in the LUBEL mutant fly lines can be overexpressed. If this causes a rescue of the phenotype, this indicates that LUBEL influences the abnormal tubulin phenotype.

Being that LUBEL has been shown to regulate the IMD pathway, other components of the Imd pathway could be affected. Tubulin staining flies that are mutants for different constituents of the Imd pathway, such as DIAP2, Dredd, and Kenny, could provide further information on if/where the tubulin abnormality is occurring in this cellular pathway.

One possible explanation for the abnormal tubulin phenotype in LUBEL-mutated flies is through a common linkage: CYLD. CYLD is a deubiquitynating enzyme (DUB) that regulates the NF-κB pathway by removing M1-ub chains from Kenny in the Imd pathway (Aalto et al., 2019).   Additionally, CYLD is composed of three cytoskeleton-associated protein glycine-rich (CAP-Gly) domains. These CAP-Gly domains have been shown to regulate microtubule (MT) dynamic and function, and more importantly, CYLD enhances tubulin polymerization into MTs by lowering the required concentration for MT assembly (Gao et al, 2008). In LUBEL-mutant flies, there is a decrease in M1-ub chain formation (Aalto et al, 2019). One hypothesis: This decrease in M1-ub chain formation could reduce the need of DUBs, such as CYLD, to regulate M1-ub chains. This could cause an excess concentration of free CYLD, which could influence MT dynamics, such as tubulin polymerization. More specifically, an increase in unbound CYLD causing an increase in tubulin polymerization, which could account for the abnormal phenotype that is seen in LUBEL-mutant flies.

5.2.2   *lubel^{Mi}* and *lubel^{RNAi}* flies have thicker dorsal trunks in comparison to the control groups.

In addition to the abnormal tubulin structures, *lubel^{Mi} and lubel^{RNAi}* flies also have a significantly thicker dorsal trunks in comparison to the control groups. These measurements were acquired by collecting three width measurements from each larval dorsal trunk and then the average dorsal width was calculated. Using the drawing tool in Fiji, a line was drawing across the dorsal trunk and the length of the line was recorded. This method was used due to its simplicity and time restraint of the project, but this measurement does not indicate if the increased dorsal trunk thickness is due to dilation of the tracheal airway, or due to increased diameter of the epithelium, which would in theory constrict the tracheal airway. Increased respiratory constriction could contribute to the fatality of *lubel^{Mi}* flies in hypoxic conditions causing asphyxiation.

For future experiments, the dorsal trunk should be imaged along the Y-axis in order to obtain an image of the trachea from the side, as if one is looking through a telescope. By acquiring this image, one could use the same method to measure the dorsal trunk width, but also measure the width of the airway to determine if there is respiratory constriction in LUBEL-mutant fly lines.

6. CONCLUSION

These findings are biologically significant to humans because *Drosophila melanogaster* are genetically orthologous to mammals, and flies have been shown to be a useful model for studying the mechanism behind airway inflammation in mammals (Roeder et all, 2011). This novel phenotype could provide insight to the mechanisms behind airway inflammation in various diseases such as asthma and COPD. This abnormal tubulin phenotype has never been seen before in our lab, and to our current understanding, has not been shown in any previous literature. This posed an enormous challenge with moving forward in the project after the discovery of this phenotype. I developed and optimized an entirely new dissection, staining, and imaging protocol in order to investigate this abnormal phenotype in *Drosophila melanogaster* larvae.

7. ACKNOWLEDGEMENTS

I would like to acknowledge all of the members of the Inflammatory Signaling Lab at Åbo Akademi University who guided and supported me during this thesis project, especially my supervisors: Annika Meinander and Anna Aalto. All of the staff at the CIC, especially Markku Saari and Ciaran Butler-Hallissey, for training and assistance with various imaging techniques and image processing. Thank you to the staff and instructors of the BIMA program, especially my teacher tutor, Diana Toivola. A special thanks to Elena Tcarenkova for assistance with STED imaging.

And lastly, I would like to dedicate this thesis to my mom, Reneé Benoit, who encouraged me to study in this program and pursue this master's degree. Without her endless support and love and encouragement, none of this would have been possible. She inspired me and gave me the courage to continue onwards even when things felt impossible.

<div align="center">

In loving memory of Reneé Odette Benoit

April 2, 1969- September 9, 2019

</div>

8. REFERENCES

Aalto, A.L., A.K. Mohan, L. Schwintzer, S. Kupka, C. Kietz, H. Walczak, M. Broemer, and A. Meinander. 2019. M1-linked ubiquitination by LUBEL is required for inflammatory responses to oral infection in *Drosophila*. *Cell Death and Differentiation.*

Abramowitz, M., and Davidson, M.W. 1999. Photomultiplier Tubes: Concepts in Digital Imaging Technology - Photomultiplier Tubes. Olympus Life Science.

Airy, G.B. 1835. On the Diffraction of an Object-glass with Circular Aperture. Transactions of the Cambridge Philosophical Society. 5:283.

Baffet, A.D., B. Benoit, J. Januschke, J. Audo, V. Gourhand, S. Roth, and A. Guichet. 2012. Drosophila tubulin-binding cofactor B is required for microtubule network formation and for cell polarity. Mol.Biol.Cell. 23:3591-3601.

Bardell, D. 2004. The Invention of the Microscope. Bios. 75:78-84.

Centanin, L., T.A. Gorr, and P. Wappner. 2010. Tracheal remodelling in response to hypoxia. *J Insect Physiol.* 56:447-454.

D'Ignazio, L., and S. Rocha. 2016. Hypoxia Induced NF-κB. *Cells.* 5.

Fister III, J.C., J.M. Harris, D. Rank, and W. Wacholtz. 1997. Molecular Photophysics of Acridine Yellow Studied by Phosphorescence and Delayed Fluorescence: An Undergraduate Physical Chemistry Experiment. *J.Chem.Educ.* 74:1208.

Ghabrial, A., S. Luschnig, M.M. Metzstein, and M.A. Krasnow. 2003. Branching morphogenesis of the Drosophila tracheal system. Annu.Rev.Cell Dev.Biol. 19:623-647.

Gines, T.B, and M.W. Davidson. 2018. Stimulated Emission Depletion (STED) Microscopy: Fundamentals. Zeiss.

Harrison, J.F. 2009. Chapter 256 - Tracheal System. In Encyclopedia of Insects (Second Edition). V.H. Resh and R.T. Cardé, editors. Academic Press, San Diego. 1011-1015.

Hayashi, S., and T. Kondo. 2018. Development and Function of the Drosophila Tracheal System. Genetics. 209:367-380.

Herman, B., Centonze, V., Frohlich, J.R., Lakowicz, D.B.M., Spring, K.R., and Davidson M.W. 2015. Molecular Expressions Microscopy Primer: Specialized Microscopy Techniques - Fluorescence - Basic Concepts in Fluorescence. The Florida State University.

Hetru, C., and J.A. Hoffmann. 2009. NF-κB in the Immune Response of *Drosophila*. *Cold Spring Harb Perspect Biol.* 1.

Jennings, B.H. 2011. *Drosophila* – a versatile model in biology & medicine. *Materials*

Today. 14:190-195.

Lakowicz, J. 2006. Principles of Fluorescence Spectroscopy.

Loganathan R., Cheng Y. L., Andrew D. J., 2016.   Organogenesis of the Drosophila respiratory system, pp. 151–211.

Lukinavičius, G., G.Y. Mitronova, S. Schnorrenberg, A.N. Butkevich, H. Barthel, V.N. Belov, and S.W. Hell. 2018. Fluorescent dyes and probes for super-resolution microscopy of microtubules and tracheoles in living cells and tissues. Chem.Sci. 9:3324-3334.

Lukinavičius, G., K. Umezawa, N. Olivier, A. Honigmann, G. Yang, T. Plass, V. Mueller, L. Reymond, I.R. Corrêa Jr, Z. Luo, C. Schultz, E.A. Lemke, P. Heppenstall, C. Eggeling, S. Manley, and K. Johnsson. 2013. A near-infrared fluorophore for live-cell super-resolution microscopy of cellular proteins. Nature Chemistry. 5:132-139.

Lukinavičius, G., L. Reymond, E. D'Este, A. Masharina, F. Göttfert, H. Ta, A. Güther, M. Fournier, S. Rizzo, H. Waldmann, C. Blaukopf, C. Sommer, D.W. Gerlich, H.D. Arndt, S.W. Hell, and K. Johnsson. 2014. Fluorogenic probes for live-cell imaging of the cytoskeleton. Nat.Methods. 11:731-733.

Mandracchia, B., X. Hua, C. Guo, J. Son, T. Urner, and S. Jia. 2020. Fast and accurate sCMOS noise correction for fluorescence microscopy. Nature Communications. 11:94.

Merzendorfer, H., and L. Zimoch. 2003. Chitin metabolism in insects: structure, function and regulation of chitin synthases and chitinases. J.Exp.Biol. 206:4393-4412.

Nielsen, M.G., S.R. Gadagkar, and L. Gutzwiller. 2010. Tubulin evolution in insects: gene duplication and subfunctionalization provide specialized isoforms in a functionally constrained gene family. BMC Evolutionary Biology. 10:113.

Pitsch, S., and Köster, I. 2015. A Bright Dye for Live-Cell STED Microscopy. Leica Microsystems.

Prasad, V., D. Semwogerere, and E. Weeks. 2007. Confocal microscopy of colloids. Journal of Physics: Condensed Matter. 19:113102.

Roeder, T., K. Isermann, and M. Kabesch. 2009. Drosophila in asthma research. Am.J.Respir.Crit.Care Med. 179:979-983.

Sanderson, M., I. Smith, I. Parker, and M. Bootman. 2014. Fluorescence Microscopy. Cold Spring Harbor Protocols. 2014.

Spit, M., E. Rieser, and H. Walczak. 2019. Linear ubiquitination at a glance. J.Cell.Sci. 132: jcs208512.

Swatek, K.N., and D. Komander. 2016. Ubiquitin modifications. Cell Res. 26:399-422.

ThermoFisher Scientific. 2017. Anatomy of Fluorescence Spectra. Molecular Probes School of Fluorescence.

Yutaka Shimizu, Lucia Taraborrelli, and Henning Walczak. 2015. Linear ubiquitination in immunity. 266:190-207.

Weaver, M., and M.A. Krasnow. 2008. Dual origin of tissue-specific progenitor cells in Drosophila tracheal remodeling. Science. 321:1496-1499.

Wong, M.M., M. Liu, and S.K. Chiu. 2015. Cropped, *Drosophila* transcription factor AP-4, controls tracheal terminal branching and cell growth. *BMC Developmental Biology.* 15:20.

8. APPENDIX

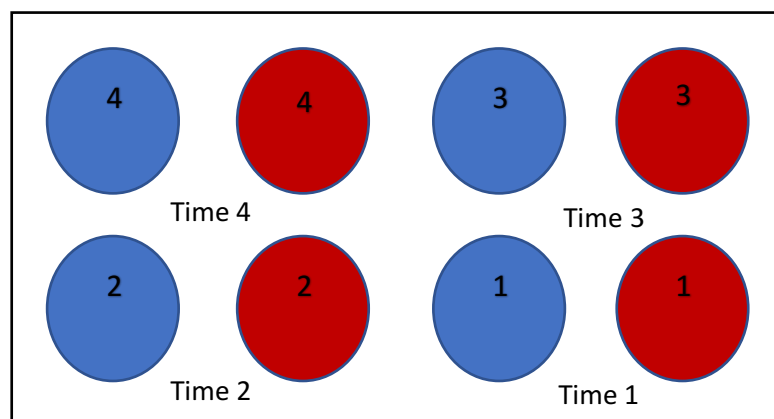# SiR-Tubulin & Calcofluor White Staining Protocol

By Sabrina Benoit

GOAL OF THIS PROTOCOL: DUAL-CHANNEL IMAGING OF DISSECTED THIRD INSTAR LARVAE TO INVESTIGATE TRACEAL MORPHOLOGY BY STAINING FOR TUBULIN AND CHITIN

> **SiR-Tubulin** → Abs/Em: 652/674 nm (compatible with Cy5)
>
> **Calcofluor White** → Abs/Em: 380/475 nm (compatible with DAPI)

PART 1: Preparation and Dissections

- Collect third instar larvae, place in -20°C for ~30 min.

- Prepare wells with 500 µL cold 1% BSA-PBS (remove BSA), add 500 µL cold 1xPBS to each well. Place wells and falcon of cold PBS in box of ice.

- Dissect larvae in cold PBS and place in prepared wells. *When nearing completion of dissections, remove SiR-T, Verapamil, and CW from -20°C (located in grey box with yellow tape) and defrost in dark @ room temp.*

An example experiment setup. *Make sure to record the time it takes to dissect each group and randomize dissection order.*

PART 2: Staining and Incubation

- Remove PBS from well, add 250 μL **staining solution**:

  - 1 μM SiR-Tubulin, 1 μM Verapamil, and 1 μM Calcofluor White in 1xPBS

  (e.g. 1 μL SiR-T and 1 μL Verapamil in 1000 μL 1xPBS). *Spin down fluorophores before use.*

  ** *Verapamil can be increased up to 3 μM if SiR-T signal is weak.*

  ***Remove PBS from well and immediately add solution to prevent drying*

- Incubate ~1.5 hr in dark @ room temp. Wrap the wells in foil and place in a drawer. *Remove Moviol from -20°C and defrost at room temp.*

PART 3: Washing and Mounting (MOST IMPORTANT PART!!)

- After incubation, prepare a new "washing well" for each "incubation well" following the preparation protocol (500 μL BSA-PBS rinse and 500 μL PBS).

  - *E.g. Looking at the earlier model, 4 groups x 2 fly lines (control and mutant) = 8 washing wells*

- Gather supplies: double-sided tape, Moviol, 70% ethanol, cotton swabs, lens paper, microscope slides (75x25 mm), #1.5 cover glass.

- Mount samples under dissection microscope, clean the stage of the microscope with ethanol and paper towel. Spray ethanol on cotton swab and clean both sides of microscope slide and cover glass, dry with lens paper. *Tape can be used to remove lingering dust particles.*

- Place 2 spacers (double-sided tape) on the microscope slide, spread 5 μL Moviol on the slide. *Be careful not to create any bubbles.*

- Remove 1 larvae from the staining solution, gently place the larvae in the washing well, wait ~10 sec, gently remove the larvae, and position the larvae with trachea facing upwards on the microscope slide. Repeat this step for all the larvae in your group (3-4 larvae can fit on one microscope slide).

  - *It is important to work quickly during this step as the larvae will begin to dry out on the microscope slide.*

- On the clean cover glass, place three drops (~4 µL/drop) of Moviol in a row. Using the forceps, align your Moviol over the larvae and gently place the cover glass over the sample.

  - *15-20 µL of Moviol per slide depending on the number of larvae*

- Seal the edges of the cover glass with clear nail polish. Allow the slides to dry for ~15 min in dark @ room temp on flat surface before imaging or storing in dark @ +4°C.

An example mounting setup. *Make sure to write experiment # and group # on slide.*
MAKE SURE YOU KNOW YOUR LARVAE!

Microscope Slide   Cover Glass

Moviol
Positioned larvae
Spacers
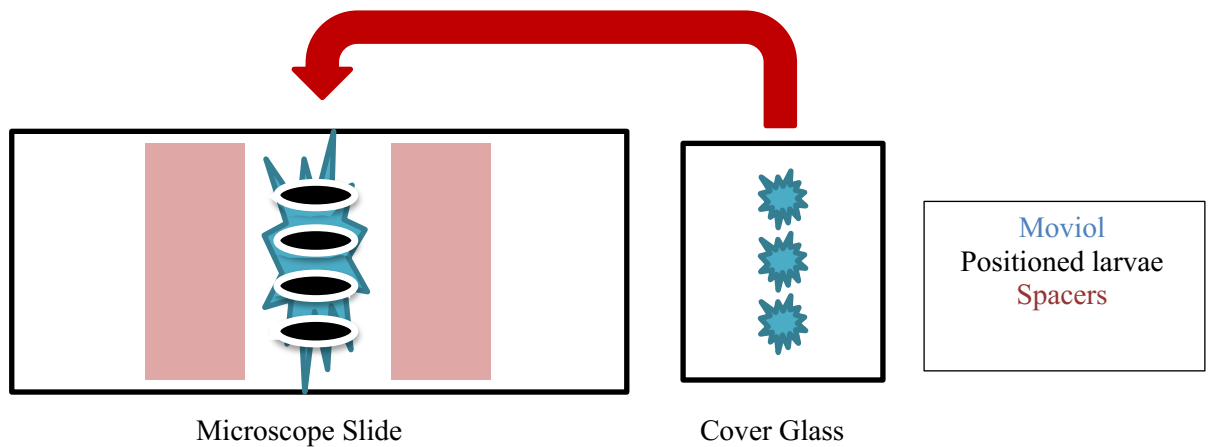
LSM 880 Imaging Guidelines and Image Processing Tips

PART 1: Preparation and Setup

- Startup system and power on lasers according to BTK user manual
- Switch to 40x mag, add drop of water to objective
- Use "Smart Setup"
    - Cy5 (red): SiR-staining- IR channel
    - Calcofluor White (blue)- UV Channel
    - FITC (green)-autofluorescence for QC
- Choose "Best Signal" → separate tracks, we want highest signal intensity
    - *Our probes are durable, so speed is less significant*

PART 2: Locate ROI and Configure Lasers

- Place microscope slide with cover glass down on the objective. Raise objective until water drop makes contact with the slide.
- Using the eyepiece and transmitted light (TL illumination), continue to raise the eyepiece to locate sample and find focal plane
    - *Start from anterior or posterior end and scan the sample until you find a representative area (ROI)*
- Check fluorescence intensity using red filter and eyepiece (RL illumination)
- Using the camera, configure one laser at a time
    - Use T-PMT + Cy5 Brightfield to find area with strong signal

PART 3: Acquisition Settings

- Use optimal frame size, unless otherwise justified
- Acquisition speed: 6-8, 9 for Z-Stack
- Averaging: at least 2, Mode: line
- Adjust laser power (2-5%), Gain (~800), and Offset (0 → -10 or more)
    - *ALWAYS SET PINHOLE TO 1 AIRY UNIT UNLESS OTHERWISE JUSTIFIED*
    - *Automated "Set Exposure" works well with Cy5*

○ ***NEVER USE AUTOFOCUS! CHECK PINHOLE SIZE AFTER AUTO EXPOSURE!***

PART 4: Z-Stack Scanning

- Use live scan to find start and end position

- Use optimal slice size (*obeys **Nyquist Sampling Theorem** - waveform is sampled over twice as fast as its highest frequency component*)

  ○ *E.g. 1.3 μm section size (found near pinhole) → 0.65 μm sampling slice size*

  ○ *Smallest scanning section = sample section*

- ***KEEP SAME SCANNING PARAMETERS FOR ALL SAMPLES!***

  ○ *Start and end position must be determined for each ROI*

PART 5: Image Processing using Fiji

- After saving images from the computer (save as original CZI) open the files in Fiji software. *Download software for free from https://fiji.sc/*

- Image – Stack – Make Z-Project…

  ○ *Choose all slides unless you have very bright exoskeleton towards top or bottom of the stack.*

  ○ Use Max. Intensity or Avg. Intensity

    ▪ *Avg. Intensity is good for images with blurry background*

- Brightness + Contrast (B&C). *Shortcut* SHIFT+C.

  ○ Adjust Maximum and Minimum

  ○ ***NEVER ADJUST BRIGHTNESS OR CONTRAST! THIS CHANGES THE ORIGINAL PIXEL VALUE OF YOUR IMAGE.***

- Analyze – Tools – Scale Bar…

  ○ *Check your unit (microns or pixels, choose microns)*

  ○ Lower right positioning, choose appropriate value (e.g. 10, 50 or 100 microns depending on objective used)

- If you want to add color to the image, apply LUT (Lookup Table). Save processed image as TIFF file

Benoit, Sabrina